Quaternary slip rates along the northeastern boundary of the Arabia-Eurasia collision zone (Kopeh Dagh Mountains, Northeast Iran)

Esmaeil Shabanian, Lionel Siame, Olivier Bellier, Lucilla Benedetti, Mohammad R. Abbassi

Geophys. J. Int. (2009) **178,** 1055–1077 doi: 10.1111/j.1365-246X.2009.04183.x

Quaternary slip rates along the northeastern boundary of the Arabia–Eurasia collision zone (Kopeh Dagh Mountains, Northeast Iran)

Esmaeil Shabanian,[1] Lionel Siame,[1] Olivier Bellier,[1] Lucilla Benedetti[1] and Mohammad R. Abbassi[2]

[1]*CEREGE – UMR CNRS, Université Aix-Marseille, IRD, Collège de France, Europôle de l'Arbois,* BP 80, 13545 *Aix-en-Provence Cedex* 4, *France. E-mail: ismael@cerege.fr*

[2]*International Institute of Earthquake Engineering and Seismology (IIEES),* BP 19395-3913 *Tehran, Iran*

Accepted 2009 March 16. Received 2009 March 13; in original form 2008 May 16

SUMMARY

The Kopeh Dagh is accommodating a large portion of the northward motion of central Iran with respect to Eurasia, involving a major right-lateral strike-slip fault system (Bakharden–Quchan). This fault system corresponds to the northeastern boundary of the Arabia–Eurasia collision, and can be considered as a lithospheric-scale tectonic feature. We present a well-constrained estimation of late Quaternary slip rates along two major strike-slip faults (the Baghan and Quchan faults) in this fault system, using *in situ*-produced ^{36}Cl nuclide to date two offset alluvial fan surfaces. Combining detailed satellite image and digital topographic data analyses complemented with geomorphic fieldwork allows quantifying the cumulative offset values of 940 ± 100 and 360 ± 50 m of the fan surfaces along the Baghan and Quchan faults, respectively. A total of 12 carbonate boulders from the fan surfaces were collected and dated. This yields minimum age of two episodes of fan abandonment at 280 ± 16 (Baghan fault) and 83 ± 4 ka (Quchan fault). Age estimates and measured offsets of the fans are consistent with respective maximum long-term fault slip rates of 2.8 ± 1.0 and 4.3 ± 0.6 mm yr^{-1} for the Baghan and Quchan faults over the Middle-Late Pleistocene. Applying the slip rates to cumulative post-folding offsets along the Baghan and Quchan faults indicates that strike-slip motion within the Kopeh Dagh may have started ∼4 Ma. This constrains the timing of a major tectonic reorganization in the Kopeh Dagh, previously recorded through Arabia–Eurasia collision between 3 and 7 Ma. At the regional scale, the sum of total cumulative strike-slip offsets is about 35–40 km, which implies a total maximum slip rate of about 9 ± 2 mm yr^{-1} in the Central-Eastern Kopeh Dagh. This is resolved to average northward and westward slip rates of ∼8 and ∼4 mm yr^{-1}, respectively, for the Western Kopeh Dagh with respect to Eurasia. Our results also suggests that the localized strike-slip faulting in the Central Kopeh Dagh can be considered as an intercontinental movement between northeast Iran and Eurasia, accommodating about 80 per cent of northward motion of central Iran with respect to Eurasia.

Key words: Seismicity and tectonics; Continental neotectonics; Continental tectonics: strike-slip and transform; Tectonics and landscape evolution.

1 INTRODUCTION

Tectonic deformations in Iran result from the Arabia–Eurasia convergence. This convergence took place by crustal shortening and strike-slip faulting in different intracontinental deformation zones, such as the Zagros, Alborz and Kopeh Dagh mountain ranges, and the active subduction zone of the Makran. The Kopeh Dagh range (Fig. 1) corresponds to the main deformation zone at the northeastern boundary of the Arabia–Eurasia collision. During the last decade, several studies carried out in the Zagros (e.g. Regard *et al*. 2004; Talebian & Jackson 2004; Authemayou *et al*. 2005; Regard *et al*. 2005; Authemayou *et al*. 2006; Bayer *et al*. 2006; Walpersdorf *et al*. 2006; Yamini-Fard *et al*. 2007) and Alborz (e.g. Axen *et al*. 2001; Jackson *et al*. 2002; Masson *et al*. 2006; Ritz *et al*. 2006), have produced a better understanding of active deformation in these zones; such detailed studies are less common in the Kopeh Dagh (e.g. Hollingsworth *et al*. 2006; Masson *et al*. 2007; Tavakoli 2007).

The northward motion of Arabia with respect to Eurasia is accommodated at a rate of 22 ± 2 mm yr^{-1} at the longitude of Bahrain (Sella *et al*. 2002; McClusky *et al*. 2003; Vernant *et al*. 2004;

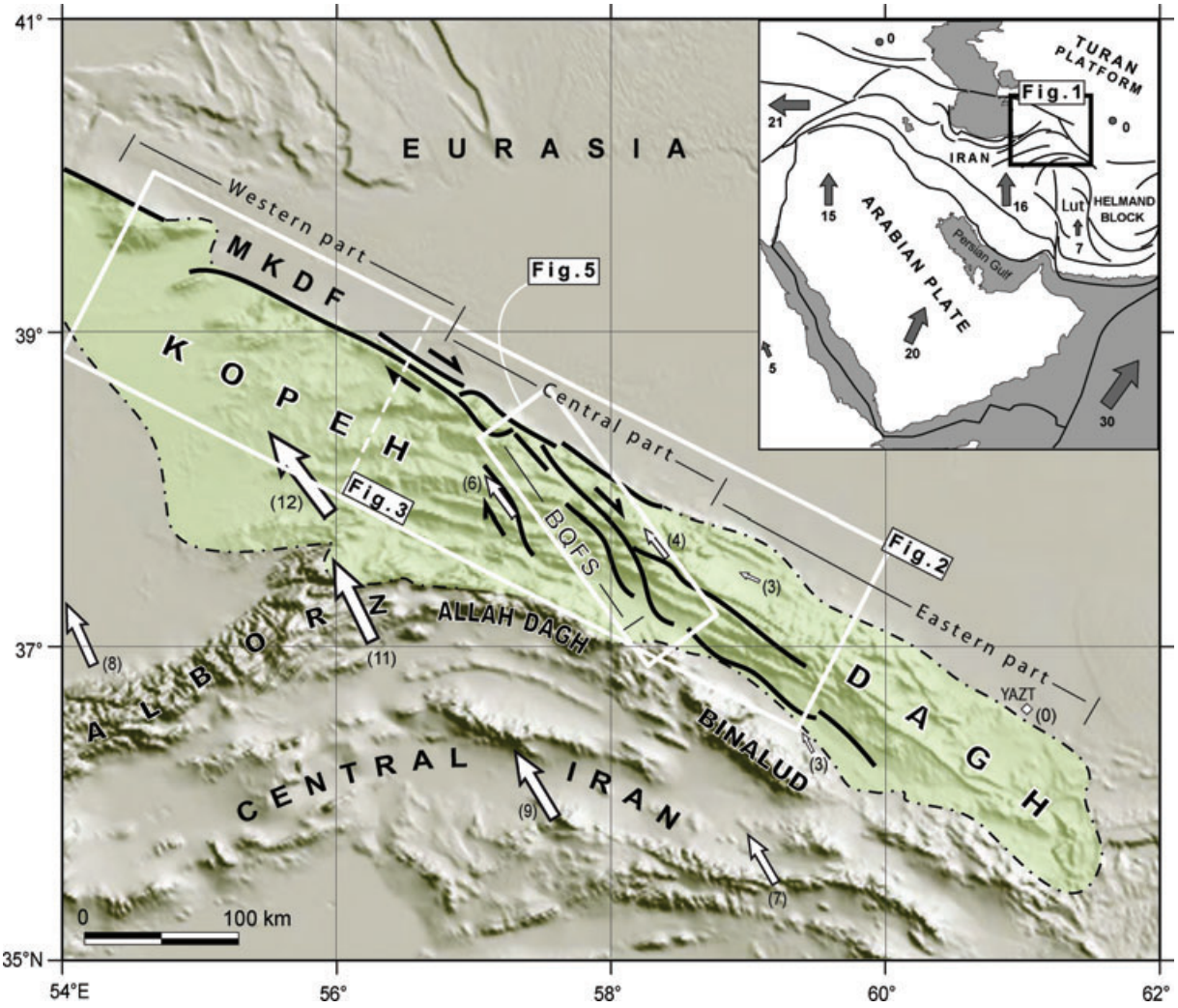

Figure 1. GTOPO30 image of northeastern Iran showing divisions of the Kopeh Dagh Mountains, the location of Bakharden–Quchan Fault System (BQFS) as well as other mountain ranges and structural units mentioned in the text. Right-lateral shear between central Iran and Eurasia is taken up on the Main Kopeh Dagh Fault (MKDF), accommodated through the Kopeh Dagh on the BQFS (black-half arrows). White arrows and associated numbers are GPS horizontal velocities in a Eurasia-fixed reference frame in millimetres per year (Tavakoli 2007). The inset with the box on the upper right shows the location in the Arabia–Eurasia collision. Grey arrows and associated numbers represent Arabia–Eurasia plate velocities. Rates are in millimetres per year (Reilinger *et al*. 2006).

Reilinger *et al*. 2006). According to the available geodetic data, this northward motion should be accommodated in northeastern Iran (mainly in the Kopeh Dagh Mountains) at a rate ranging from 4 to 10 mm yr^{-1} (Vernant *et al*. 2004; Reilinger *et al*. 2006; Masson *et al*. 2007; Tavakoli 2007), given angular relationships between block motions and major structures (Fig. 1).

The Kopeh Dagh Mountains form a NW–SE active belt separating central Iran from Eurasia (Turan platform) (Fig. 1). This mountain range accommodates a significant part of the Arabia–Eurasia convergence not absorbed by the Makran subduction (Vernant *et al*. 2004), involving thrust faulting, left-lateral strike-slip (on minor faults) in the Western, and right-lateral strike-slip in the Central-Eastern Kopeh Dagh (Afshar Harb 1979; Jackson & McKenzie 1984) mainly accommodated along a large intracontinental fault system.

In the Kopeh Dagh, the fault slip rates have been estimated using approaches spanning very different time scales: the short-term (a few years) from geodetic analysis (Vernant *et al*. 2004; Masson *et al*. 2007; Tavakoli 2007), and the long-term (∼5 Myr), using geological data (Afshar Harb 1979; Lyberis *et al*. 1998; Lyberis & Manby 1999). Geodetic measurements give access to short-term, almost instantaneous rates that include both inter- and post-seismic deformation (Tapponnier *et al*. 2001). Such short-term rates are integrated over the last several years, and long-term geological slip rates do not necessarily need to be identical, especially if strain build-up varies through the seismic cycle and on larger time scales (e.g. Dixon *et al*. 2003; Friedrich *et al*. 2003). Despite the geodynamic constraints brought by the previous studies, those may integrate different tectonic regimes and consequently variations of the slip rates. Detailed geomorphic data on fault activity is thus essential to better constrain the slip rates over the last several tens- to hundreds-of-thousands of years along the Arabia–Eurasia collision boundary in northeastern Iran, to fill the huge gap of time between geological and geodetic data sets.

This paper presents the first well-constrained estimation of Late Quaternary slip rates in the Kopeh Dagh Mountains, combining *in situ*-produced ^{36}Cl exposure dating, detailed satellite image (Landsat and SPOT) analyses, and geomorphic field surveys. After a

review of the geological setting and structural framework of the Kopeh Dagh Mountains, we present the active faulting evidence along the main fault system (Bakharden–Quchan Fault) within this mountain belt. Then, we describe the morpho-tectonic investigations conducted along two major strike-slip fault segments (Baghan and Quchan faults), allowing us determining individual Quaternary fault slip rates on the order of several millimetres per year. Our results imply that the Kopeh Dagh region has accommodated the deformation due to the collision between Arabia and Eurasia at a rate of roughly 9 ± 2 mm yr^{-1}, suggesting that the Bakharden–Quchan Fault System can be considered as an intercontinental boundary between Iranian microplate and Eurasia, accommodating about 80 per cent of northward motion of central Iran with respect to Eurasia. Moreover, analysing post-folding brittle deformation combined with the obtained fault slip rates leads to our estimate that the strike-slip faulting within the Kopeh Dagh Mountains began roughly 4 Ma.

2 GEOLOGICAL SETTING AND STRUCTURAL FRAMEWORK

The Kopeh Dagh range forms a 600-km-long and up to 200-km-wide mountain belt between the Eurasian plate (Turan platform) to the North and the Iranian block to the South (Fig. 1). It includes 10–17 km thick, Mesozoic and Tertiary sediments, which were folded during the Oligo-Miocene orogenic movements (Stöcklin 1968; Afshar Harb 1979; Lyberis & Manby 1999). The emergence of the Kopeh Dagh has been diachronous, getting younger from the eastern toward the western part of the mountain range (Afshar Harb 1979; Lyberis & Manby 1999). Folding of the Mesozoic-Tertiary sedimentary rocks after the Miocene period indicates the closure of the Kopeh Dagh basin, and emplacement of the Kopeh Dagh Mountains as a consequence of the northward motion of the Arabian shield towards Eurasia (Afshar Harb 1979; Lyberis *et al*. 1998; Lyberis & Manby 1999). Kopeh Dagh deformation accommodates part of the convergence between the Turan platform to the North and the Lut-central Iran blocks to the South.

In the northwest, the Kopeh Dagh range is bounded by the Main Kopeh Dagh Fault System (MKDF) which has been named either the 'Main Fault Zone' (Tchalenko 1975), the 'main Kopeh-Dagh fault' (Trifonov 1978), or the 'Ashgabat fault' (Lyberis & Manby 1999). This 350 km long fault corresponds to a fundamental, inherited basement structure (Amurskiy 1971; Maggi *et al*. 2000) forming the NE margin of the Kopeh Dagh as the boundary between Iran and Turan platform, and is considered as a seismically active structure (Trifonov 1978). The width of the MKDF ranges from ~6 km, northeast of Kizyl-Arvat, to ~20 km southwest of Bakharden, where it is intersected by the post-Miocene Bakharden–Quchan Fault System (BQFS; Figs 1 and 2). This particular region has been suggested as the southeastern limit of the clear surface expression of the MKDF (Hollingsworth *et al*. 2006).

The BQFS is constituted by active NNW-trending, right-lateral strike-slip fault segments dissecting the Central-Eastern part of the Kopeh Dagh range (Fig. 1). This fault system extends between the MKDF to the North, and the Binalud range, which can be regarded as the northern margin of central Iran to the South. The BQFS

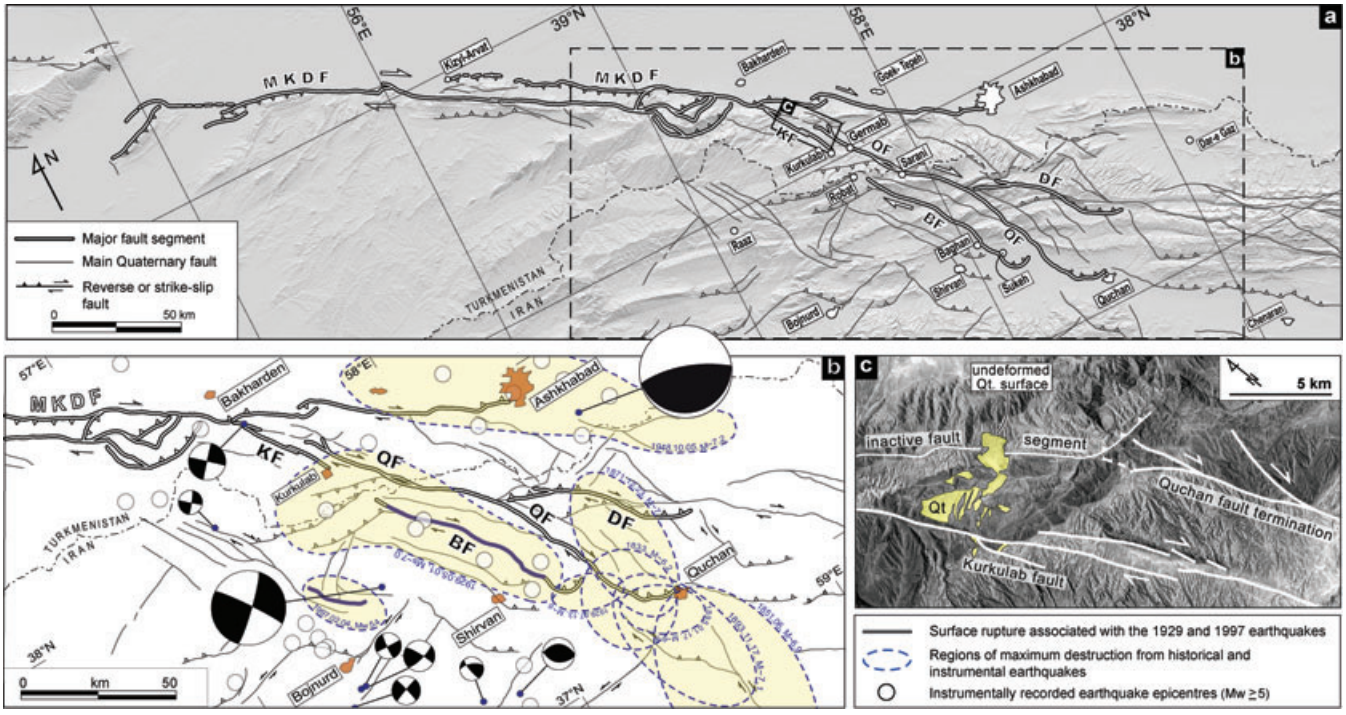

Figure 2. (a) Detailed Quaternary fault map of the Central-Eastern Kopeh Dagh and the Main Kopeh Dagh Fault system, including recognized Quaternary faults with a length longer than 10 km (prepared in this study). Two rectangles marked by b and c are the region of (b) and (c). Abbreviations are as follows: MKDF, Main Kopeh Dagh Fault; KF, Kurkulab Fault; QF, Quchan Fault; BF, Baghan Fault; DF, Dorbadam Fault. (b) Historical and instrumental seismicity of the Kopeh Dagh. Focal mechanisms are mainly taken from the Harvard catalogue (http://www.globalcmt.org/CMTsearch.html) and McKenzie (1972). Epicentres are from the NEIC catalogue (http://neic.usgs.gov/neis/epic/epic_global.html). The regions of maximum destruction are mainly based on Tchalenko (1975) and Ambraseys & Melville (1982), with one of the 4th February 1997 Garmkhan earthquake from Hollingsworth *et al*. (2007). Thick-black lines are surface ruptures associated with the 1929 Baghan (Tchalenko 1975) and 1997 Garmkhan (Hollingsworth *et al*. 2007) earthquakes. (c) LANDSAT image of the Kurkulab-Quchan relay fault zone; the Quaternary trace of the Quchan fault terminates as it splits into a horse-tail structure.

is the surface expression of basement faults with a considerable cumulative lateral displacement at the surface (Amurskiy 1971; Tchalenko 1975; Afshar Harb 1979). The lack of basement steps (gravity survey, Amurskiy 1971) along these faults suggests also a predominance of lateral movements at depth. Combining the results of recent geodetic and geodynamic studies (Vernant *et al*. 2004; Reilinger *et al*. 2006; Masson *et al*. 2007; Tavakoli 2007) as well as seismicity distribution, with large cumulative geomorphic (this study) and geological feature offsets (e.g. Afshar Harb 1979; Afshar Harb *et al*. 1987) observed along the BQFS, strongly implies that the BQFS can be interpreted as a continuation of the eastern Iran boundary, allowing central Iran to move northward with respect to Afghanistan, as a part of Eurasia (Jackson & McKenzie 1984; Vernant *et al*. 2004).

3 ACTIVE FAULTING ALONG THE BQFS

The BQFS is composed of 10 major, roughly parallel, NNW-trending faults or fault zones with individual segment lengths ranging from 40 to 140 km, corresponding to a 45-km-wide band of transpressive deformation (Figs 1 and 2). Most of the fault segments were mapped on regional scale geological maps (Huber 1977; Afshar Harb *et al*. 1980; Afshar Harb 1982; Afshar Harb *et al*. 1987). Both on digital topography and satellite imagery, their parallel and straight surface traces indicate an array of nearly vertical faults (Fig. 2).

In the northwest, the BQFS bends into the MKDF without clear evidence of crosscutting relationships, which indicates the merging of the both fault systems (Fig. 2). Along the southern limit of the BQFS, the fault zone expression is not conspicuous but it may terminate in the Kashafrud-Atrak Valley between the Kopeh Dagh and Binalud mountain ranges (Hollingsworth *et al*. 2006).

In this study, analyses of satellite images combined with digital topographic SRTM data and direct field observations allowed us to investigate active faulting along the BQFS. Two different resolutions of satellite images (Landsat ETM+ and SPOT5 with pixel size of 14 and 5 m, respectively) were used for regional mapping. The entire fault system is mapped in detail with special attention to the relay zones and intersection points between different fault segments. This allows distinguishing, on a geometric and geomorphic basis, fault segments representative of the dominant structural pattern. Fig. 2 presents all the recognized Quaternary fault segments with a length longer than 10 km. Among the 10 individual main Quaternary faults and fault zones in the BQFS, the Baghan Fault and the Kurkulab-Quchan Fault zone (KQF) are considered as the two principal structures. The next two sections provide a set of short-term ($\sim 10^2$ yr) and long-term ($\sim 10^6$ yr) evidence to consider the KQF and the Baghan Fault as the major active structures in the Kopeh Dagh Mountains.

3.1 Instrumental and historical seismicity in the Kopeh Dagh Mountains

A long and detailed historical record of earthquakes in northeast Iran spans over the last 900 yr (Tchalenko 1975; Ambraseys & Melville 1982; Berberian & Yeats 1999; Berberian & Yeats 2001). Along the BQFS, the relationship between seismicity and fault segments has already been discussed by Tchalenko (1975) and Ambraseys & Melville (1982), and recently re-evaluated by Hollingsworth *et al*. (2006) for modern large earthquakes in the western part of the region. Since the 19th century, the Kopeh Dagh region has experienced at least 12 large earthquakes with magnitudes ranging from 6.5 to 7.5, and almost all of those seismic events occurred in the vicinity of the BQFS (Fig. 2). In this context, the Baghan and Quchan faults are responsible for at least six of these large earthquakes [Baghan earthquake: 1929; Quchan earthquakes: 1851(?), 1871–1872, 1893, 1895; Tchalenko 1975; Ambraseys & Melville 1982]. When considering the macroseismic regions associated to these historical earthquakes, the band of maximum destruction appears to follow the trends of the Quchan and Baghan faults. There is no evidence for such seismicity along the other structures in this zone. This supports the major role of the Quchan and Baghan faults within seismogenic behaviour of the Central-Eastern Kopeh Dagh.

3.2 Distribution of cumulative geological offsets in the Kopeh Dagh Mountains

To understand and quantify the contribution of the BQFS to the accommodation of the Quaternary deformation at a regional scale, distribution of post-folding brittle deformation in the Kopeh Dagh was carefully examined using satellite imagery, SRTM data and field observations (Fig. 3). This analyses allowed us investigating detailed morphologies, total offset measurements, as well as the structural linkage between the different fault segments. At the regional scale, there is no geomorphic or geological evidence for a significant vertical component along the major strike-slip faults over the whole BQFS. This is in agreement with a predominance of lateral movements at depth (Amurskiy 1971), as well as focal mechanism data (Fig. 2). In addition, according to our field observations, a fault rake (slip-vector on fault plane) ranging from 0° to 10° (Fig. 4) can be considered as a characteristic value for strike-slip motions in the Kopeh Dagh. Taking this characteristic fault rake into account, a maximum vertical displacement on each fault segment might not exceed by 11 per cent the associated lateral displacement. According to these observations, cumulative post-folding horizontal displacements can be measured directly on satellite images, thanks to parallel fold axes and well-stratified geological formations offset by strike-slip faults.

The cumulative displacements measured along the BQFS segments range from 100 m to 18 km (see the Appendix). Those measurements are presented as displacement isolines at a regional scale (Fig. 3), allowing us distinguishing the structural importance of each individual fault segment in the region. The northeastern part of the region is occupied by the Turan platform where there is no deformation (Fig. 3). The largest portions of strike-slip movements are localized on the MKDF and the BQFS. Among the investigated faults, the KQF and the Baghan Fault are the most important ones, exhibiting maximum cumulative displacements of $\sim$15 and $\sim$10 km, respectively (Afshar Harb 1979; Afshar Harb *et al*. 1987; Hollingsworth *et al*. 2006). As a result, the combined observations of large post-folding offsets and occurrence of major destructive earthquakes during the last three centuries, suggest that the KQF and the Baghan Fault can be considered as the major strike-slip faults and consequently the main seismogenic sources in the Kopeh Dagh Mountains.

3.3 The Kurkulab–Quchan fault zone

The longest fault zone in the BQFS system is constituted by two major fault segments which connect the MKDF to the northern limit of the Binalud fault system (Fig. 2). This fault zone was previously considered to be the Quchan Fault (Hollingsworth *et al*. 2006).

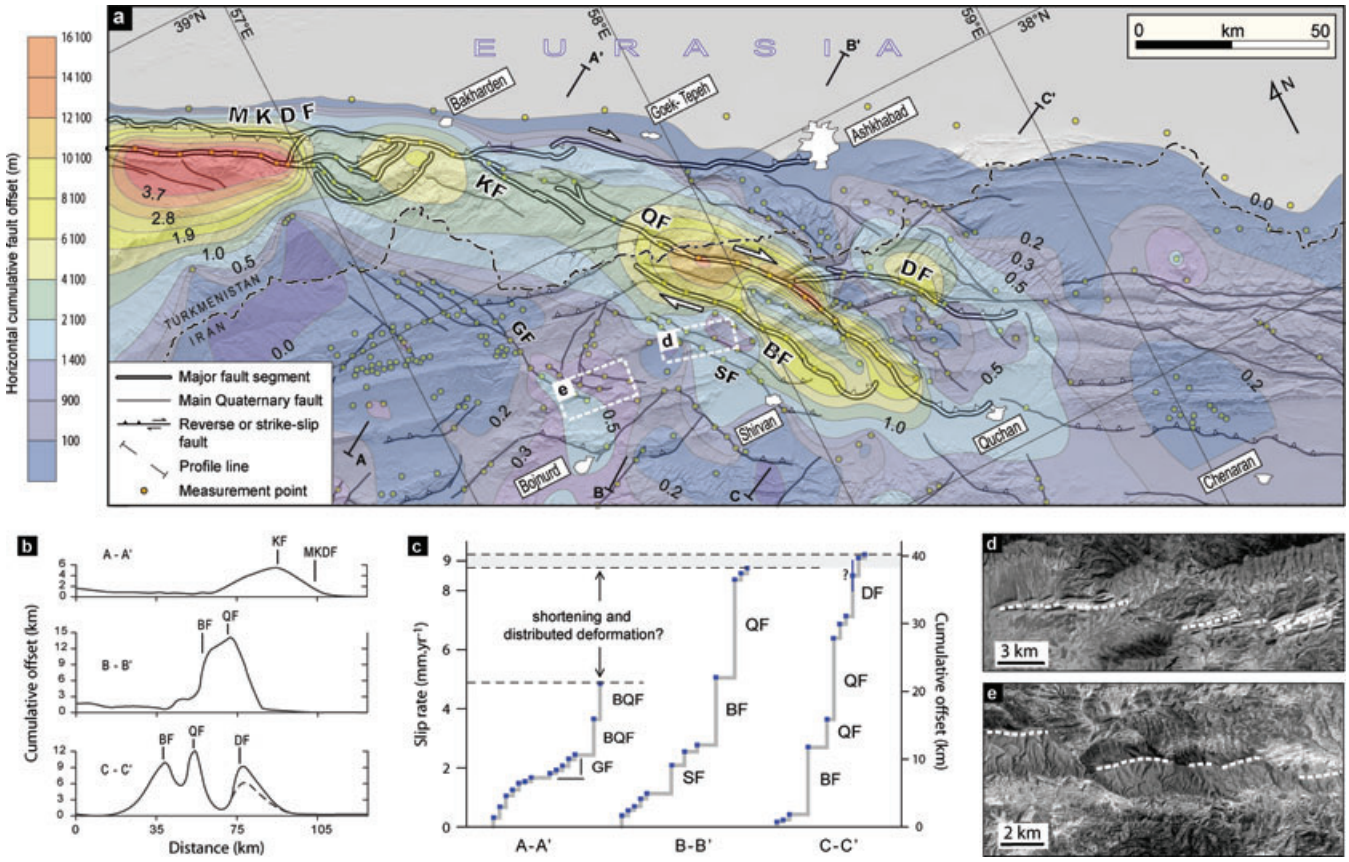

Figure 3. (a) Regional distribution of cumulative strike-slip offsets (filled contours) and their equivalent long-term slip rates (numbered contours) in the Kopeh Dagh Mountains. Slip rates are expressed in millimetres per year. GF, Gholaman Fault zone; SF, Shirvan Fault; other abbreviations as the caption of Fig. 2. (b) Profiles along which distribution pattern of the cumulative geological offsets is presented through the Kopeh Dagh Mountains. Location of profiles is marked on (a). It should be noted that the cumulative offset on the DF (<10 km) is undifferentiated sum of right-lateral displacement (the probable dotted line: ~6 km) and apparent offset due to oblique thrust faulting with respect to fold axes. (c) Total slip rates for paths A–A', B–B' and C–C' shown in (a). (d) And (e) SPOT5 image of the southern part of the GF and SF, respectively, two examples for cumulative geological offsets analysed in this study.

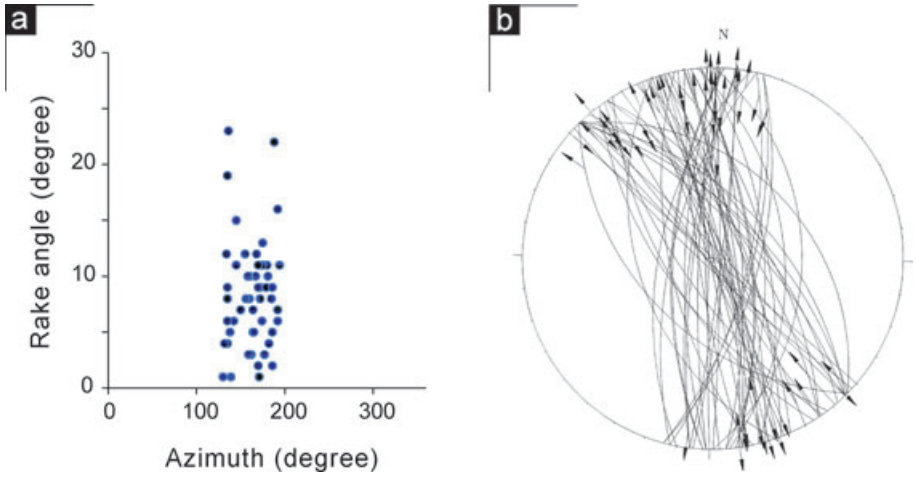

Figure 4. Fault plane data indicating a characteristic rake value ranging from 1 to 10° for strike-slip faults within the Kopeh Dagh Mountains. (a) Fault rake angle versus fault azimuth. (b) Stereographic projection of the fault data including fault striations.

However, even if the Quchan Fault connects to the MKDF, there is no direct Quaternary structural linkage between these two fault zones. On the basis of our observations, we propose the name of KQF for this complex structure.

The Quchan Fault is the longest segment of the KQF, which is the largest strike-slip fault zone in the BQFS. The Quchan Fault extends from the city of Quchan in the southeast to 24 km north of Germab village in the northwest (Fig. 2). As characteristic features, displaced geomorphic markers such as alluvial fans, beheaded drainages and offset active streambeds, indicate Quaternary activity along much of its length. More to the north, the Quaternary trace of the fault terminates as it splits into a horsetail structure (Fig. 2). The ancient

trace of the main fault is conspicuous on satellite image and digital topography, and runs northward about 2 km beyond this area, where it is covered by an uplifted Quaternary terrace that is not affected by the fault trace (Fig. 2c). On the basis of our observations, the northern termination of the Quchan Fault is a relay zone between two major fault segments of the BQFS. The Kurkulab Fault runs between the relay zone and the MKDF continuing the BQFS to the North, turning obliquely into the MKDF (Fig. 2). Hereafter, we pay a special attention to the structural and geomorphic characteristics of the Quchan Fault.

3.4 The Quchan fault

Although Quchan Fault can be mapped continuously from Quchan up to 134 km northwards and the northern termination can be clearly delineated, the southern limit is less clear. However, subtle geomorphic evidences indicating its thrust-bend termination in the Atrak Valley (Fig. 5) have been described near the city of Quchan by Hollingsworth *et al*. (2006). The Quchan Fault obliquely cuts the Oligo-Miocene folds of the Kopeh Dagh with a maximum right-lateral offsets of ∼15 km in the folded bedrock (Fig. 5). The strike of the fault segment does not varies much, except southeast of Sarani village, where the Quchan Fault rotates anticlockwise by ∼27° along a 25-km-long restraining bend (Fig. 5). This particular area is characterized by rotation and dragging in both morphological and structural features, and probably represents an old short-cut zone between two distinct fault segments.

In the case of the Quchan Fault, aside from fault tip terminations, the main prominent structural complexities are the intersection points of the main fault with other fault traces. The Owghaz and Bey-Bahreh faults are two parallel, strike-slip faults with a maximum length of roughly 50 km, which intersect the Quchan Fault (Fig. 5). These faults displace the bedrock in clear right-lateral offsets (of about 2 km) east and west of the main structure. Due to this structural arrangement, maximum offset of the major fault corresponds to the sum of total offsets along the three faults within the intersection zone (Fig. 5).

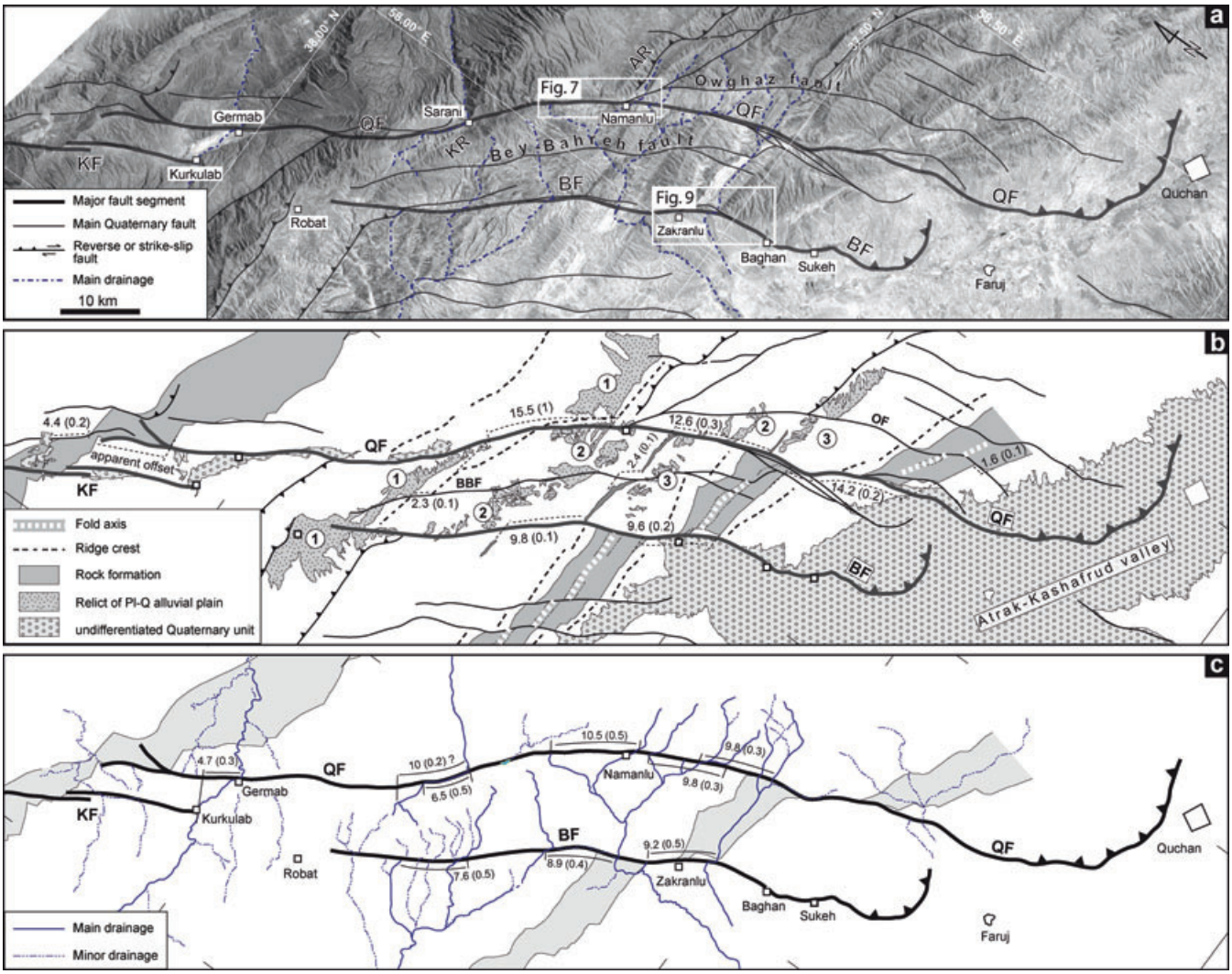

Figure 5. (a) LANDSAT image of the BQFS indicating detailed 2-D geometry of the Quchan and Baghan faults and their associated right-lateral offsets in the folded bedrock as well as undeformed linear markers such as anticline axes and ridge crests. AR, Agh-Kamar Ridge; KR, Konjukhor Ridge. (b) Morphotectonic map of the BQFS based on (a). The values of cumulative geological offsets are presented as numbers with their associated uncertainties in parenthesis. Corresponding relict alluvial plains have been marked by the same numbers (1–3) beside the faults. (c) Cumulative geomorphic offsets on the BQFS. The offset values are expressed in kilometres.

In this area of the Kopeh Dagh, several rivers flow across the Quchan Fault. The river courses follow synclinal axes parallel to the belt, and incise through growing anticlines (Fig. 5). Assuming that those rivers initiated during the same period of time, they can be used to compare contemporaneous offsets along the fault traces. A maximum cumulative, right-lateral offset of about 10 km can be measured on the Southern and Central parts of the Quchan Fault, while this value decreases northward to roughly 5 km, near of Germab (Fig. 5). This observation is in agreement with a northward termination of the Quchan Fault in the relay zone, where the fault trace is covered by a non-deformed Quaternary terrace (Section 3.3).

3.5 The Baghan fault

With a length of 80 km, the Baghan Fault runs northwest between Sukeh village on the northern bank of the Kashafrud Valley, and Robat village at the border between Iran and Turkmenistan (Fig. 5). The Baghan Fault trends exactly parallel to the Quchan Fault as a single fault segment, so the perpendicular distance between the two faults (an average of ∼11 km) is constant along strike (Fig. 5). This common geometry probably indicates a structural inheritance in the basement and/or a rheological effect of different geological formations affected by the faults.

The Baghan Fault is responsible for the 1929 Baghan earthquake (Ms ∼7) that was associated with a 50-km-long coseismic ground rupture (Tchalenko *et al*. 1974; Tchalenko 1975; Ambraseys & Melville 1982). Tchalenko (1975) described a SE-facing fault scarp, visible from place to place as a 2 m high, rounded topographical step (or 1 m according to Ambraseys & Melville 1982). Comparing total length of the Baghan Fault (80 km) with this 50-km-long coseismic ground rupture (Fig. 2), indicates that only 60 per cent of the whole length of the fault may have been reactivated during the 1929 Baghan earthquake. The Baghan Fault is characterized by kilometric geological displacements to metric geomorphologic offsets that can be observed both on satellite images and in the field (e.g. Tchalenko 1975; Afshar Harb 1979). Among those features, the river network that flows north across the Baghan Fault is right-laterally displaced by a maximum of 9 km (Fig. 5).

4 MORPHO-TECTONIC INVESTIGATIONS

4.1 Methodologies

4.1.1 Geomorphic mapping and site selection

At the site scale, analyses of SPOT5 images combined with aerial photographs, and direct field observations were used to quantify geomorphic offsets along the recognized active fault segments. Among several possibilities, we selected two key sites offering several advantages for understanding the displacement history of the Quchan and Baghan faults: (1) Maximum total offset on a single fault strand, (2) well-preserved alluvial fans offset by the fault, providing readily datable markers and constrained fault offset values and (3) small catchment basins close to the alluvial fans to minimize inheritance of *in situ*-produced cosmogenic ^{36}Cl in our samples. The first studied site is located close to Namanlu village (Fig. 5), on an alluvial fan which is offset by the Quchan Fault (Fig. 7). At this particular location, we also surveyed several thousand topographic data points (∼86 000 x, y, z points) using Leica 530 post-processing kinematic (PPK) GPS, to provide a large-scale digital elevation model of the fan surface. The second site is a large alluvial fan located close to Zakranlu village (Fig. 5), and affected by the Baghan Fault.

4.1.2 Sampling and estimating surface exposure ages

On the two offset fan surfaces, both the geomorphic setting and the surface characteristics were carefully considered in selecting boulders to be sampled. For both the Namanlu and Zakranlu surfaces, limestone boulders (>50 cm) embedded on their surfaces were sampled avoiding angular, visibly broken and non-rooted boulders. Considering exponential drop off *in situ*-produced ^{36}Cl concentrations with respect to sampling depth, spalled boulder surfaces were avoided, and samples were collected from the upper 1–8 cm on top of boulders. Additionally, there is no evidence that the boulders might have been moved and/or buried before their exposition at the present surface. Most of the sampled boulders are characterized by carbonate collars (e.g. McFadden *et al*. 1998) covering the bottom of the boulders (Fig. 6), supporting that the sampled boulders were embedded at the fan surfaces for relatively long span of time. In fact, carbonate collars are relatively abundant in pavements associated with alluvial fans of various ages formed on limestone-rich alluvium. Overland flows and locally extensive surface erosion by sheet flow (Wells *et al*. 1985, 1987; McDonald, 1994) would likely limit or preclude carbonate collar formation. In addition, any subaerially exposition of carbonate collars should also dissolve such precipitates quickly (McFadden *et al*. 1998). In other words, the formation of these carbonate collars implies a long-term stability of the fan surface, and a long residence of the boulders at the surface. According to McFadden *et al*. (1998), in areas currently favourable to vesicular horizon (Av) formation, this horizon (and its associated collars) must have formed at times before the Holocene during similarly arid conditions.

For all the sampled sites, the shielding by the surrounding topography, snow cover, and sample geometry are found to be of negligible impact on the surface production rates. The watersheds identified to be the source areas of the sampled alluvial fans are rather short and steep catchments, implying short transport times and little along-stream storage. This particular geomorphic situation allows minimizing inheritance of *in situ*-produced cosmogenic ^{36}Cl in our samples. For the Namanlu alluvial fan, the sampled surfaces are located away from recent incision rills, and show a relatively fresh morphology (Fig. 6). For the Zakranlu (Honameh) alluvial fan(s), the region today is under traditional dry-farming cultivation but these activities had little effects on the initial morphology of the fan surface (Fig. 6).

Considering that, on such abandoned surfaces, erosion cannot be expected to be uniform, either temporally or spatially (e.g. Fig. 6), erosional effects on the boulder exposure ages were minimized by carefully analysing the geomorphic setting and the surface characteristics of the alluvial fans. In this context, the most preserved parts of the fan surfaces were selected for sampling (Fig. 6). Preserved morphology of the selected parts of the fan surfaces indicates a trivial influence of erosion on these sampled parts. Although we suspect that little erosion of the surfaces may have occurred, any erosion would render our ages as minima. That is, the actual exposure ages of the surface may be older than the cosmogenic ages we report herein. In the following discussions, all of our exposure ages are minima, even though we think that the true abandonment ages may be close to the sample ages (due to the absence of surface runoff and lateral transport). We note however, in the following discussion

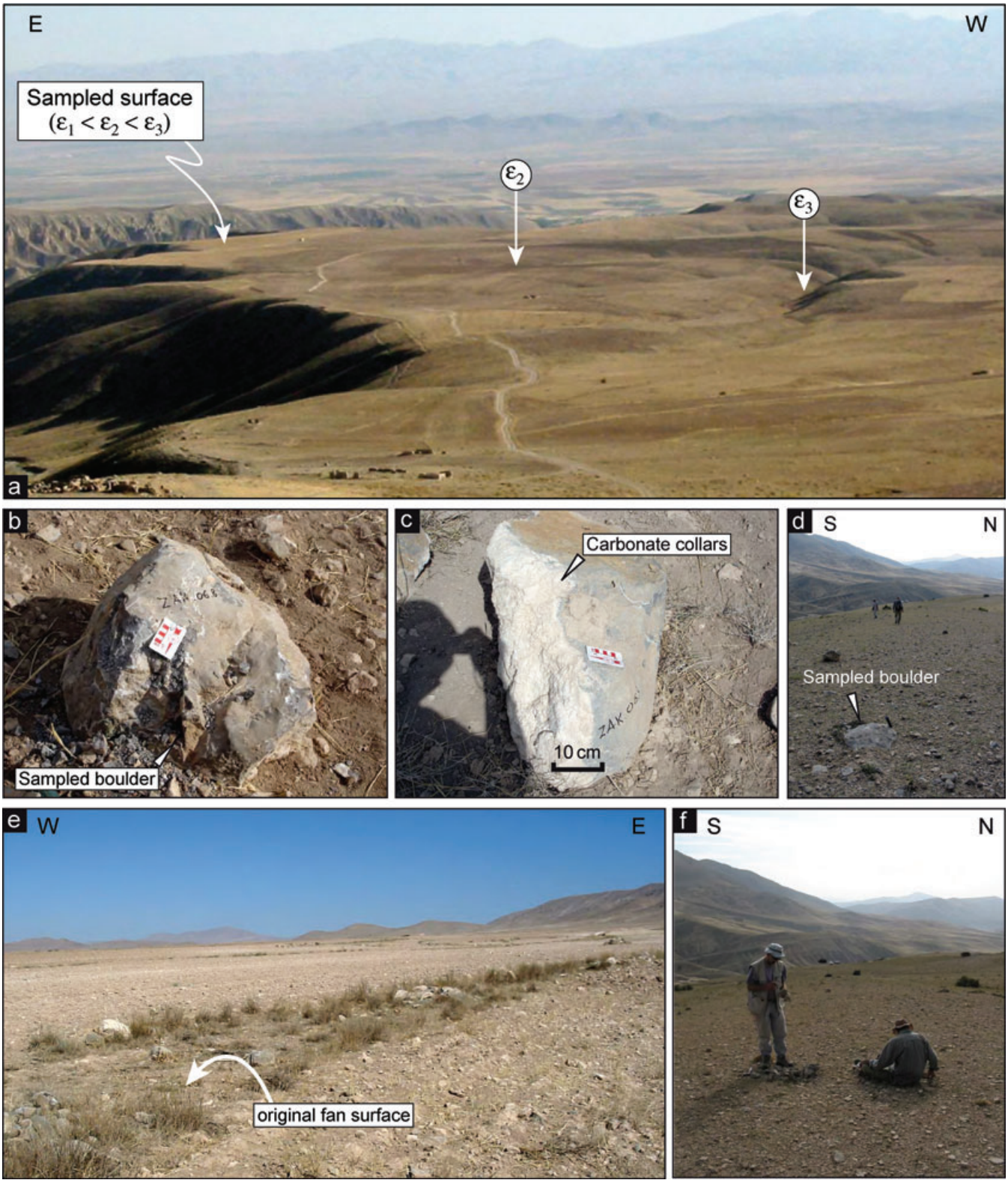

Figure 6. (a) General view of the Zakranlu fan surface, taken from the fan apex, showing non-uniform erosion (ε, whatever the involved mechanism) on the different parts of the fan surface. The most preserved part of the surface was sampled. (b) Typical carbonate boulder sampled on the Zakranlu fan surface. (c) An example of characteristic carbonate collars on the embedded parts of the sampled boulders. This boulder was exhumed by the field team after sampling in order to demonstrate the degree of carbonate collar development typical of the samples embedded in the fan surface. (d) And (f) General view of the relatively well-preserved sampled part of the Namanlu fan surface. (e) Insignificant effect of traditional dry-farming cultivation on the initial morphology of the Zakranlu fan surface (darker part of the surface).

that because our cosmogenic ages provide minimum abandonment ages (and initiation of offset) of the fan surfaces, that all the slip rates we discuss below should be considered maximum rates.

To date the sampled boulders, we used the *in situ*-produced ^{36}Cl cosmogenic exposure dating method. The systematic of *in situ*-production of cosmogenic nuclides is described within the review paper by Gosse & Phillips (2001). One can also refer to Stone *et al*. (1996), Stone *et al*. (1998) and Schimmelpfennig *et al*. (2009) for *in situ*-produced ^{36}Cl specifically. The treatment of the samples, such as grinding, leaching and chemical extraction of chlorine by precipitation of silver chloride, was performed following the methodology described by Stone *et al*. (1996). The ^{36}Cl and chloride concentrations in the carbonate were determined for all samples by isotope dilution accelerator mass spectrometry (AMS) at the Lawrence Livermore National Laboratory's CAMS. Blank was two orders of magnitude lower than the samples and replicates were within less than 5 per cent.

Chlorine-36 has multiple production pathways, which include spallation reactions (Ca, K, Ti and Fe), capture of low-energy epithermal and thermal neutrons (^{35}Cl), and direct capture of slow negative muons (^{40}Ca and ^{39}K). Moreover, the radiogenic ^{36}Cl must be evaluated by measuring uranium and thorium concentrations in the target mineral (Bierman *et al*. 1995; Stone *et al*. 1998; Gosse & Phillips 2001; Schimmelpfennig *et al*. 2009). It is therefore important to know precisely the chemical composition of the target mineral to determine the rate of production (see hereafter), and thus correctly interpret the measured ^{36}Cl concentrations. Major elemental composition of rock samples was determined by ICP-OES technique. The boulder ages were calculated using the Ca concentrations in the dissolved part of the samples (target fraction) according to Schimmelpfennig *et al*. (2009). The production rates proposed by Stone *et al*. (1998) were found more appropriate with respect to other production rates measured in whole-rock content (e.g. Phillips *et al*. 1996). Indeed, Stone *et al*. (1998) production rates were calibrated using calcium-rich mineral separates in which the spallation production mechanism from calcium is dominant. The rates were corrected for elevation and latitude using the correction factors from Stone (2000). To illustrate cosmogenic-derived minimum exposure age data and their associated uncertainties, we used the sum of the Gaussian probability distributions (e.g. Deino & Potts 1992), already used by different authors for dating purposes (e.g. Lowell 1995; Daëron *et al*. 2004), according to (e.g. Taylor 1997)

$$p_{\mathrm{sum}}(t) = \sum_i \mathrm{e}^{-(t-a_i)^2/2\sigma_i^2}/\sigma_i\sqrt{2\pi},$$

where t is time, a_i is the exposure age of sample i and $(2\sigma_i)$ is the reported error. A probability value less than 0.05 indicates that there is a significant amount of non-analytical error in the data set, and that one or more samples are outliers. In such a case, cumulative frequency plots are generally bimodal in shape, with the secondary peak identifying outliers.

4.2 Morpho-tectonic investigations along the Quchan Fault

Along its whole length, the Quchan Fault offsets geomorphic landforms such as Quaternary alluvial fans, fluvial plains and drainage channels at different observation scales (Figs 5 and 7). The Quchan Fault exhibits a convincing right-lateral offset of ∼15 km marked by a linear mountain ridge, made up of Cretaceous limestone. Located close to the junction of the Quchan and Owghaz faults (Fig. 5), this offset corresponds to the maximum observed post-folding displacement along the Quchan Fault trace. In this area, a ∼16 km-long, west-facing fault escarpment was caused by dragging and stretching of the limestone ridge parallel to the fault, separating the Agh-Kamar and Konjukhor ridges in eastern and western fault blocks, respectively (Fig. 5). The fault escarpment prepared a suitable condition to form several post-offset talus and alluvial fans, which have been cut during the Late Quaternary fault activity. Among these Quaternary landforms, the Namanlu alluvial fan is one of the best geomorphic features providing favourable conditions for both surface exposure dating and measurements of cumulative displacements (Fig. 7). Crossing the Namanlu fan, the fault is characterized by a relatively narrow, 110–150-m-wide fault zone. The Namanlu fan is comprised of a single fan surface and there is no evidence for post-offset successive depositions onto the fan surface. These observations suggest that no aggradation episode has occurred since the fan surface was abandoned. Therefore, considering the fan location, narrowness of the fault zone and relatively well-preserved fan surface, the Namanlu fan provides an excellent opportunity to estimate the late Quaternary slip rate of the Quchan Fault.

4.2.1 Cumulative offset recorded by the Namanlu fan

The Namanlu fan border is strongly incised by drainages, and several landslides distributed around the edge of the fan have modified its initial shape (Figs 7 and 8). Within this context, the present-day fan shape does not permit to accurately measure the actual fault offset. To measure the cumulative horizontal offset recorded by the Namanlu fan, we used two different methods. The first method consists of aligning the deformed axial trace of the fan on both sides of the fault to reconstruct the initial fan axis. The second method compares different centres of concentric topographic contour lines on the fan surface in order to locate the initial apex point. To apply the first method, several transverse topographic profiles were used to reconstruct the initial shape of the fan axis (Fig. 7). Along such profiles, the fan surface envelope forms an upward convex curve where its highest part corresponds to the fan axis. However, in regions of active tectonics, this classic shape can be tilted or deformed due to both vertical and horizontal displacements. In such cases, regardless symmetry of the profiles, areas of maximum amplitude (in comparison with the initial base) represent the axis area (Fig. 7). Plotting on the fan surface the identified axial areas, results in illustrating the cumulative deformation of the fan axis, caused by lateral fault motions. On the Namanlu fan, thanks to the high-resolution topographic survey, fourteen topographic profiles, with horizontal intervals of about 80 m, were analysed across the fan to determine the exact position of the fan axis (Fig. 7). The reconstruction of initial fan axis represents a cumulative right-lateral offset of 340 ± 40 m along the Quchan Fault. The uncertainty accounts for the average length of the planar part of the fan axis area along each topographic profile.

To apply the second method, one can also make the assumption that topographic contour lines are concentric arcs having their curvature centres located at the fan apex. Fitting alluvial fan contours with circular arcs; one can thus reconstruct the fan radii and thus determine the location of the fan apex at the time of deposition (e.g. Keller *et al*. 2000, and references herein). Due to this geometry, lateral offsets appear as different centres which are aligned parallel to the fault, while, tilting or vertical offsets can be identified as different centres shifted across the fault, respecting angle of tilting and fault dip. Using this method, the fan toe

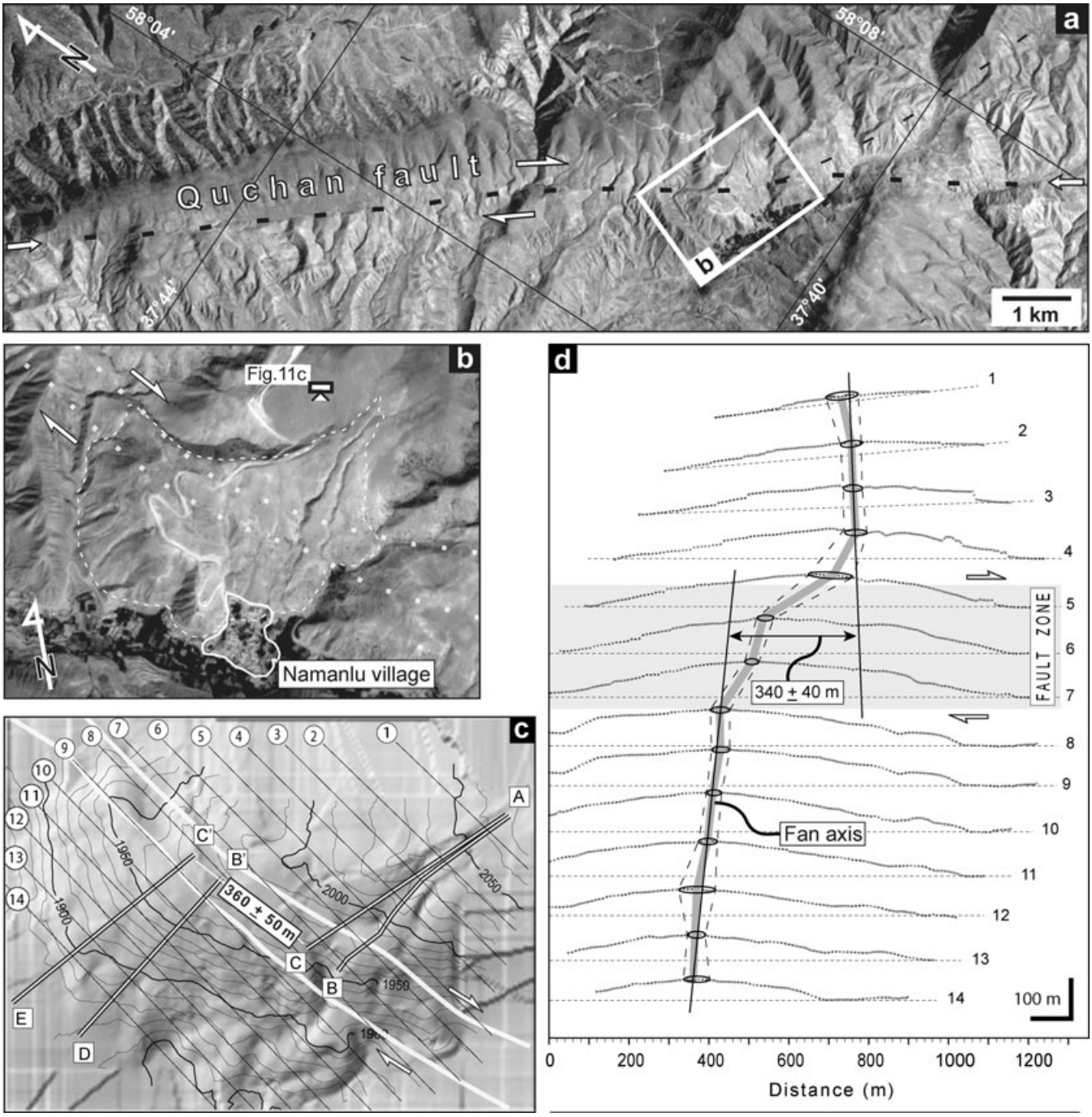

Figure 7. (a) And (b) SPOT5 image of the Namanlu alluvial fan at two different scales. The Namanlu fan has been deformed along the Quchan Fault (dotted lines in b). (c) Differential GPS-derived DEM of the fan (constituted by 85663 x, y, z points). Numbered lines indicate transverse topographic profiles used to reconstruct the initial shape of the fan axis. Double lines are the location of longitudinal profiles plotted in Fig. 8(b), respecting the restored offset value of 360 ± 50 m. (d) The accurate position of the Namanlu fan axis, reconstructed analysing fourteen topographic profiles across the fan. The reconstruction of initial fan axis indicates a cumulative right-lateral offset of 340 ± 40 m along the Quchan Fault.

contours project back to a different centre than that of present-day fan head contours (Fig. 8), which is considered as representative of the horizontal displacement accumulated by the Namanlu fan. This fan shape reconstruction yields to a right-lateral offset of 380 ± 20 m for the toe with respect to the apex of the Namanlu fan (Fig. 8). Both approaches yield similar values that permit to calculate a mean cumulative right-lateral offset of 360 ± 50 m on the Quchan Fault.

As mentioned above, observed offsets along the Quchan Fault are mainly horizontal. However, a minor vertical component offset has been observed along the fault. Cumulative vertical offsets coeval with horizontal offsets are usually more complicated to estimate using displaced geomorphic markers. For obliquely offset alluvial fans (due to oblique-slip fault motions), it is necessary to restore the cumulative lateral offset of the fan before making longitudinal profiles on the fan surface. Vertical offset of the fan is then

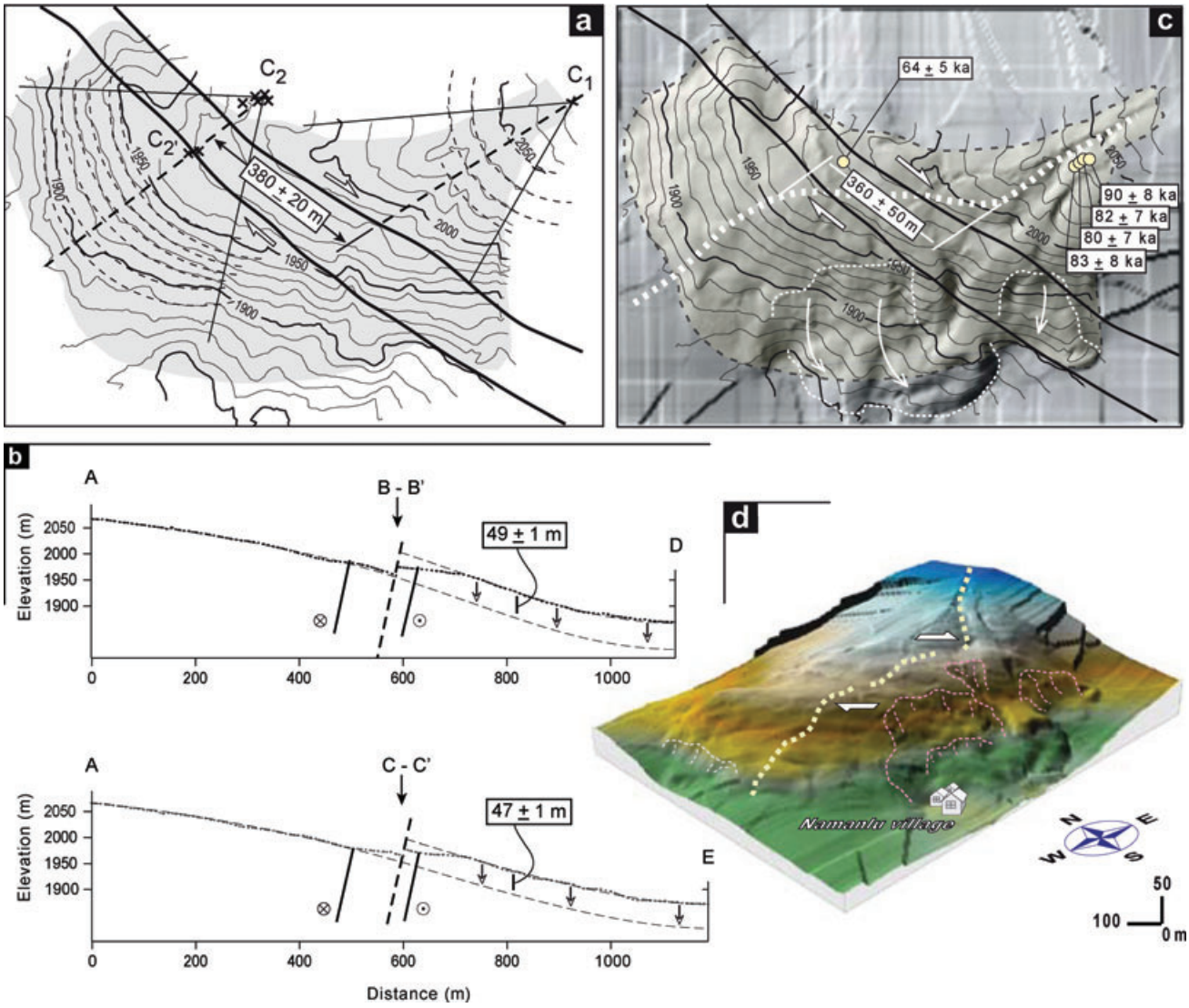

Figure 8. (a) Geometric analysis of the Namanlu fan using the concentric-contour lines method (Keller *et al*. 2000) indicates a right-lateral offset of 380 ± 20 m along the Quchan Fault. (b) Topographic profiles along the fan axis exhibiting a vertical offset of 48 ± 2 m on the Namanlu fan surface. (c) Superimposed DGPS-derived topographic and shaded relief maps of the fan indicating general morphology of the fan, reconstructed fan axis (thick, white dashed line), and landslides (thin, white dashed line) distributed around the edge of the fan. Sampling location and associated *in situ*-produced ^{36}Cl ages are shown in this figure. (d) 3-D view of the Namanlu fan.

represented by the difference in elevation between two corresponding surfaces on both sides of the fault. To do so, we used the previously described horizontal offset of the Namanlu alluvial fan to reconstruct the initial fan shape, and then, we produced two longitudinal profiles along and parallel to the actual fan axis, revealing a 48 ± 2 m-high, NE-facing vertical offset (Fig. 8).

In summary, the Namanlu alluvial fan has been displaced right-laterally by 360 ± 50 m and vertically by 48 ± 2 m, that is, the horizontal component is approximately seven times higher than the vertical one. This ratio of estimated horizontal and vertical displacements implies a rake (slip-vector) value of 8 ± 1°SE on a vertical fault plane.

4.3 Morpho-tectonic investigations along the Baghan Fault

Along the Baghan Fault, the most common geomorphic feature offsets are provided by drainage systems such as riverbeds and terraces, which are clearly displaced by the fault. A set of spectacular geomorphologic features can be observed in the Honameh region (Fig. 9), between the deserted village of Zakranlu and Baghan village along the southern half of the fault trace, where several alluvial fan systems and the major Karganeh River have been involved in the Quaternary history of the Baghan Fault.

In the Honameh region (Fig. 9), a sharp contrast between the piedmont and the mountain range developed due to large right-lateral offsets along the Baghan Fault. This west-facing, 600-m-high strike-slip fault escarpment is incised by a transverse drainage system running to the west (Fig. 9). These drainages are displaced or beheaded by the Baghan Fault, showing systematic lateral offset ranging from about 4 m, for the recent gullies, to 10 km for the main drainages.

Reconstructions of Mid-to Late-Pleistocene alluvial fans developed in the outlet of drainages offset by the Baghan Fault can be use to restore dextral offset along this fault. Analyses of SPOT5 images combined with direct field observations allow identifying at least

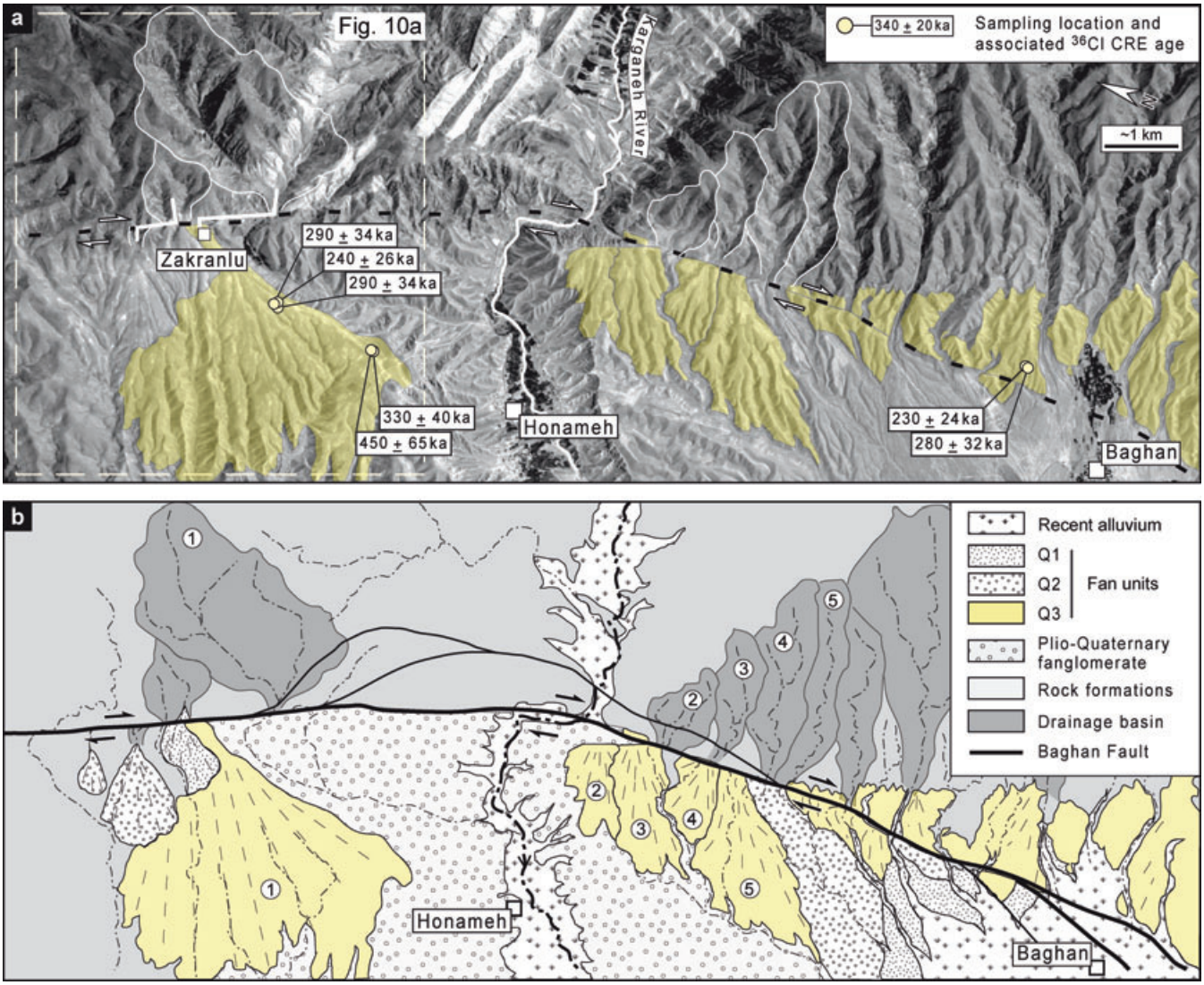

Figure 9. (a) SPOT5 image of the Honameh region including the Zakranlu alluvial fan (within dashed rectangle), Karganeh River and other geomorphic features offset along the Baghan Fault. Sharp mountain front in this region is due to cumulative right-lateral offsets along the Baghan Fault. (b) Morphotectonic map of the Honameh region based on SPOT5 image (above) and field observations. At least three abandoned alluvial fan surfaces have been offset along the Baghan Fault. Five fans (marked by numbers in circle) belonging to the Q3 unit are presently disconnected from their original feeding basins.

three main abandoned alluvial fan surfaces overlaying older Early Quaternary fanglomerates sourced from the main river (Fig. 9). The Q3 unit corresponds to alluvial fan surfaces which are essentially more incised, but not more elevated than the two other surface generations. The Q2 unit is an intermediate fan generation, which is inset in/or partially covers the Q3 unit, and exhibits preserved fan shapes. The Q1 unit corresponds to the youngest, abandoned alluvial fan surfaces, that can be observed at the toe of the two other fan generations or covering the Q3 unit south and north of the Karganeh River, respectively. Between these three alluvial fan units, the intermediate and oldest ones are right-laterally offset several hundred metres (roughly 550 and 950 m, respectively) from their feeding drainage basin situated in the other side of the Baghan Fault. They are now completely disconnected from the basins (Fig. 9). We focused our study on the Q3 fan surfaces, which are associated with a cumulative horizontal offset of up to 1 km along the Baghan Fault (Fig. 11).

South of the Karganeh River, there are at least six Q3 alluvial fan systems. Four of them have been separated from their corresponding drainage basins by right-lateral motions along the Baghan Fault. North of the Karganeh River, the Zakranlu fan is the only one belonging to the Q3 unit that is offset by the Baghan Fault (Figs 9 and 10). This characteristic avoids misinterpretation of the fault offset that may arise from uncertainty in geomorphic correlation of the fan bodies and their possible associated basins. In addition, the Zakranlu alluvial fan represents the largest and best preserved Q3 fan having approximately held its initial geometric form (Figs 9 and 10). Consequently, it is well suited for constraining a cumulative, post-Q3 abandonment, right-lateral offset along the Baghan Fault.

4.3.1 Offset of the Zakranlu alluvial fan

Fig. 9 presents a morphotectonic map of the Honameh region based on SPOT5 satellite image and field observations. To measure the cumulative offset recorded by the Zakranlu alluvial fan, its eroded apex must be reconstructed. To do so, two different methods were applied: a geomorphic method, in which the former fan shape can

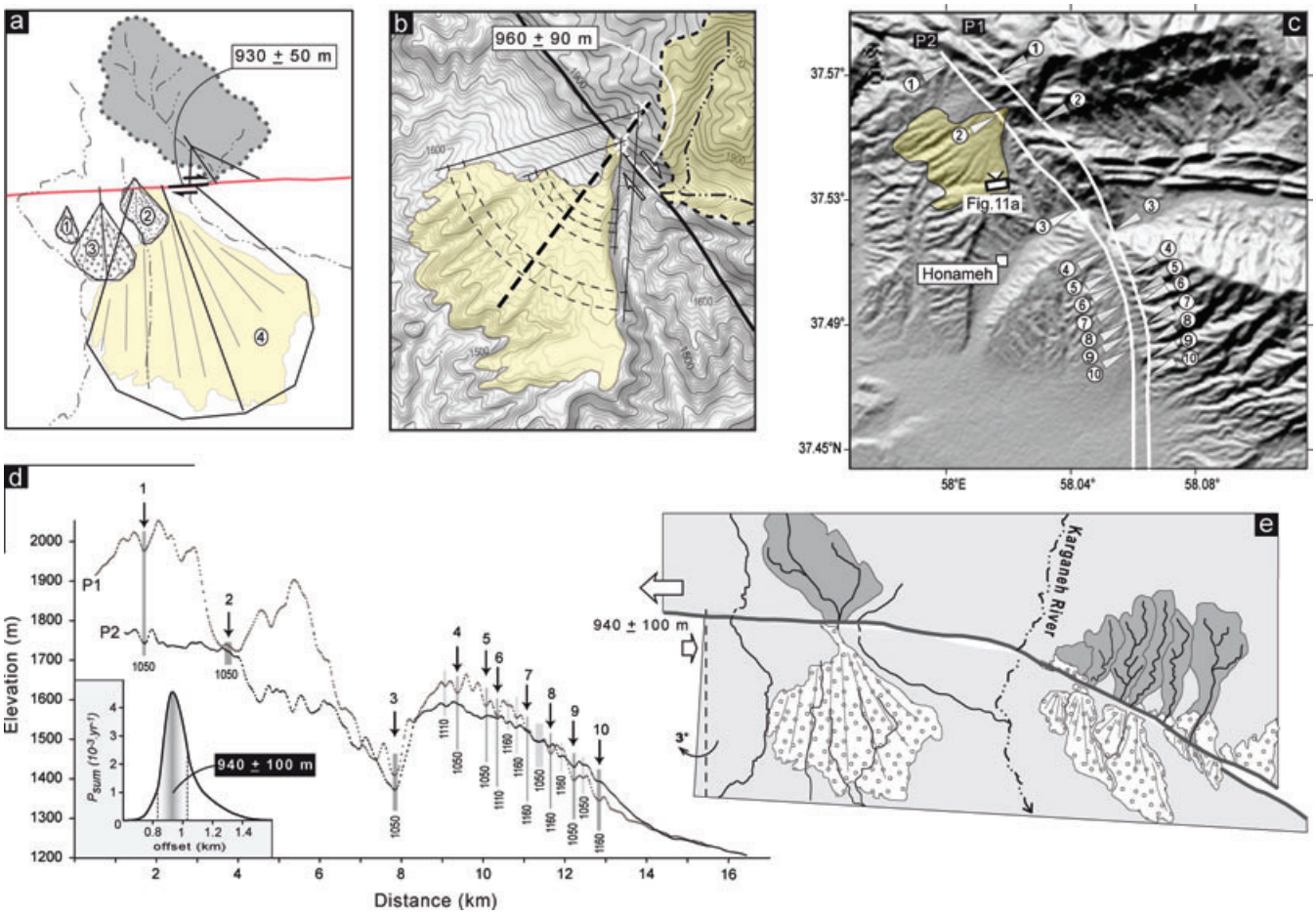

Figure 10. Applied methods to quantify cumulative offset of the Zakranlu fan: (a) Assuming that the three different fan generations in the Zakranlu fan area were developed in the same physical conditions; the initial shape of the fan was reconstructed. (b) Determining the displaced fan apex using the geometric method. (c) Shaded relief map of the Honameh region based on SRTM digital topographic data. White lines are the paths of two topographic profiles parallel to the Baghan Fault, plotted in (d). Corresponding geomorphic features beside the fault trace are marked by numbers. (d) Reconstruction of morphotectonic features along the Baghan Fault. Numbered arrows correspond to the feature numbers in (c). Corresponding offset value for each individually reconstructed feature is expressed in metres below the curves. Inset indicates the Normal probability sum of the cumulative offsets representing a constrained offset value of 940 ± 100 m. (e) Preferred reconstruction of Q3 surfaces and other contemporaneous offset features restoring the offset value of 940 ± 100 m.

be reconstructed using the remaining fan shape and its convergence slope-lines (Fig. 10); and the concentric topographic contour method described in Section 4.2.1. To complete the geomorphic method, we assumed that the three different fan generations, observed in the Zakranlu area, were developed in the same physical conditions such as piedmont slope, tectonic regime and fault mechanism. It is noteworthy that whatever the age and the size, all these fans have a similar geometric shape, denoting a common factor controlling their evolution (Figs 9 and 10). This assumption allows considering that the observed shape is a characteristic of the alluvial fans in the studied region, regardless of size and age. This leads to reconstruct the initial form of the Zakranlu fan indicating that the apex is right-laterally offset by 930 ± 50 m with respect to its former associated basin outlet along the Baghan Fault (Figs 10 and 11).

Applying the analysis of concentric topographic contours, we obtained an offset value of 960 ± 90 m that is close to the value derived from the geomorphic method but with a larger uncertainty. In fact, larger uncertainty in the geometric method is due to the sum of technical resolution of SRTM elevation data and geometric uncertainty in the location of the fan axis. However, the consistency between the results suggests reliability of the offset value regardless of the methods. Considering the two determined values, a mean cumulative right-lateral offset value of 940 ± 100 m can be calculated for the Baghan Fault since emplacement and abandonment of the Zakranlu alluvial fan.

4.3.2 Consistency of contemporaneity of Q3 fan surface offsets

To verify the reliability of the Zakranlu offset, we examined spatial consistency of the observed fault offsets affecting Q3 surfaces in the Honameh region (Fig. 10). Applying all along the fault trace the horizontal offset of 940 ± 100 m measured for the Zakranlu fan, allows a convincing restoration of the simultaneous Late Quaternary landforms such as the Karganeh River (Fig. 10). To allow this reconstruction, we assumed the same age for both the Karganeh valley in this part of its length, main drainages and all of the four displaced Q3 alluvial fans located south of the Karganeh River. In addition, random and irregular distances between the fan apexes or the basin outlets imply few possibilities to reconstruct the initial arrangement of the fan systems (Figs 9 and 10).

Another way to verify the consistency of the measured cumulative lateral offset along the Baghan Fault is to restore separately

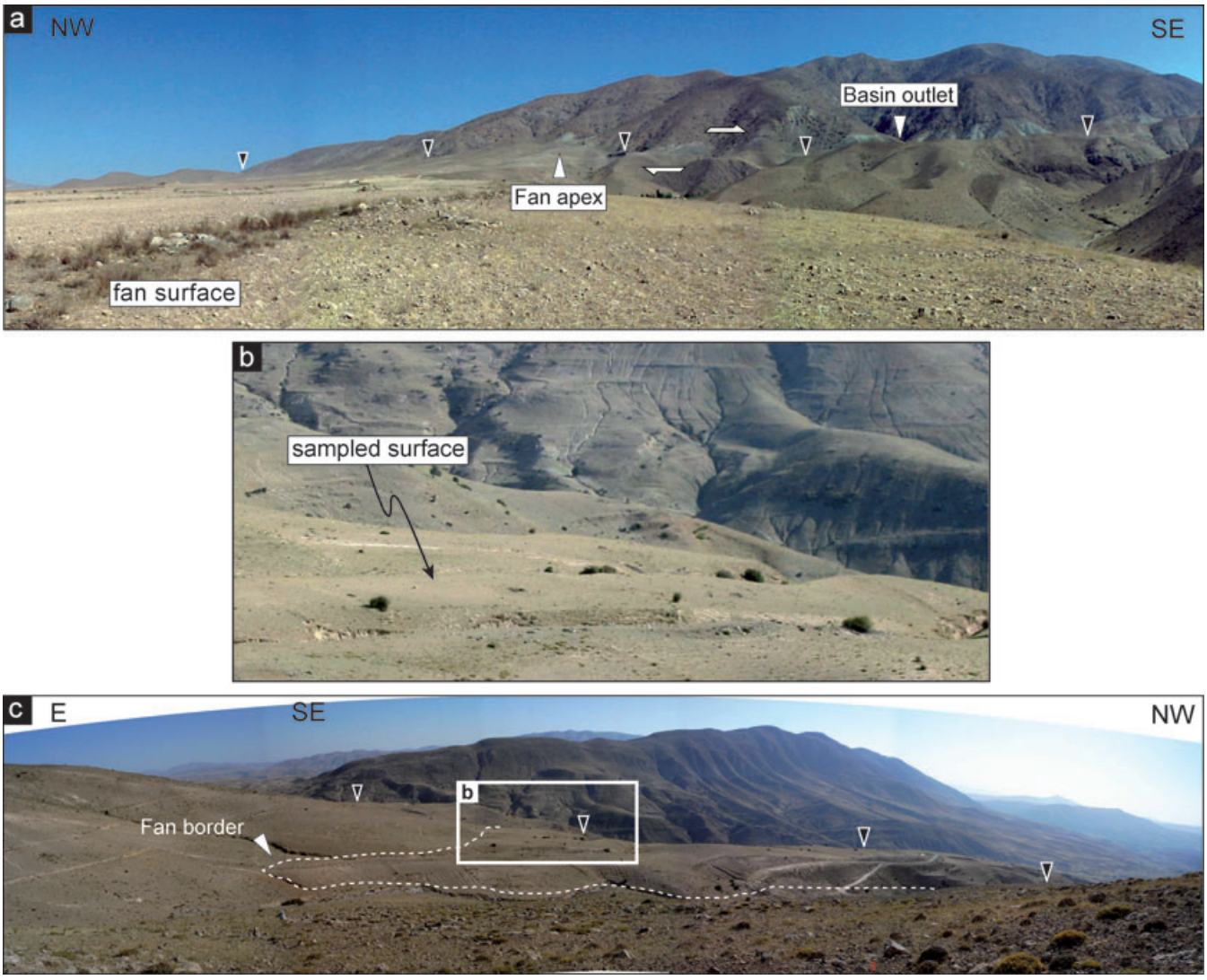

Figure 11. (a) Panoramic view of the Zakranlu fan and its catchment basin, taken from a distance of ∼2 km, the photography location was marked on Fig. 10(c). (b) The most preserved part of the Namanlu fan surface selected to be sampled; the frame of this view was marked on (c). (c) Panoramic view of the proximal part of the Namanlu fan surface, taken from a distance of ∼1 km marked on Fig. 7(b). Its distal part is hidden behind the Baghan fault scarp. Black triangles on (a) and (c) indicate the trace of the Baghan and Quchan faults, respectively.

lateral offset of each individual geomorphic element, using two topographic profiles parallel to the fault trace (Fig. 10d). The profiles were chosen to be as close as possible to the fault trace, to decrease uncertainties caused by the cosine effect of non-perpendicular objects with respect to the fault trace. Among the main geomorphic landforms (Fig. 10c), six elements out of 10 are aligned after 1050 ± 90 m of lateral back-slip along the Baghan Fault. Comparing the obtained values from both geomorphic and topographic methods indicates a good consistency of the right-lateral offset value of 940 ± 100 m, representative of the Baghan Fault cumulative offset since the emplacement of Q3.

4.4 Dating of the studied offset alluvial fans

On the Namanlu fan surface, six boulders were analysed, among which one of them was not dated at the final state (AMS measurement). These carbonate boulders embedded in the fan surface were collected from the most preserved parts of the alluvial fan surface (Figs 8 and 11). Four samples out of six were collected from the proximal part and the two others from the middle part of the fan, between two fault strands (Fig. 8). Within collected boulders, measured *in situ*-produced cosmogenic ^{36}Cl concentrations allow calculating minimum boulder exposure ages ranging between 64 ± 6 and 90 ± 8 kyr (Table 1, Fig. 8). For the Namanlu surface samples, the sum of the Gaussian age probability distributions (P_{sum}) shows a relatively sharp-peaked distribution (Fig. 12), which corresponds to a small value of σ (e.g. Taylor 1997). The minimum exposure age of the sample from the surface between the two fault strands (NAM-9) is only slightly smaller than the weighted-mean age of the boulders. This difference is indicated as a slight step-like peak in the left part of the curve (Fig. 12). Since the Namanlu fan is completely isolated and there is no evidence of successive depositions onto the fan surface, the younger exposure age of NAM-9, with respect to the principal age peak, can be interpreted as an outlier resulting from post-abandonment exhumation of the boulder within the fault zone. When considered all together (but NAM-9), the surface samples collected on the Namanlu fan surface yield a weighted-mean ^{36}Cl minimum exposure age of

Table 1. Sample characteristics and exposure ages.

Sample	Latitude (°N)	Altitude (m)	Thickness (cm)	Ca/(g rock) (per cent)	Chlorine (ppm)	^{36}Cl [atoms (g rock)$^{-1}$]	^{36}Cl production rate [atoms (g rock)$^{-1}$ yr^{-1}]	Age (kyr)
BAG16	37,47	1337	5	33,6	159,8	12 445 351 ± 150 058	59,9	283 ± 32
BAG17	37,47	1337	3	32,6	164,4	11 783 860 ± 269 762	65,5	232 ± 24
NAM1	37,68	2084	5	36,2	86,8	6721 881 ± 110 768	88,9	83 ± 8
NAM2	37,68	2084	3	35,4	122,3	7110 103 ± 95 266	87,2	90 ± 8
NAM3	37,68	2083	5	33,8	161,3	7114 060 ± 148 307	95,4	82 ± 7
NAM4	37,68	2080	7	36,3	121,9	6789 294 ± 103 179	92,5	80 ± 7
NAM9	37,68	1989	12	34,1	70,6	4667 172 ± 69 984	78,4	64 ± 6
ZAK17	37,54	1600	7	34,8	81,3	14601 738 ± 175272	63,6	326 ± 40
ZAK18	37,54	1601	2	34,8	88,7	17819540 ± 198 713	63,7	448 ± 65
ZAK19	37,55	1659	6	34,9	62,3	14 262 743 ± 158 884	67,1	292 ± 34
ZAK20	37,55	1659	7	34,8	105,4	13 837 007 ± 221 580	74,1	244 ± 26
ZAK22	37,55	1658	11	35,6	63,7	13 405 045 ± 153 424	63,7	288 ± 34

Elemental composition (per cent)

	Water	Al_2O_3	CaO	Fe_2O_3	K_2O	MgO	MnO	Na_2O	P_2O_5	SiO_2	TiO_2	Th	U
BAG16	0,12	0,90	52,89	0,25	0,05	0,76	0,02	0,01	0,04	1,52	0,03	<3	<2
BAG17	0,00	1,38	52,54	0,37	0,09	1,02	0,02	0,00	0,03	1,89	0,04	<3	<2
NAM1	0,08	1,01	54,01	0,13	0,02	0,58	0,00	0,01	0,01	1,82	0,03	<3	<2
NAM2	0,16	1,08	53,30	0,22	0,04	0,55	0,00	0,01	0,02	2,34	0,04	<3	<2
NAM3	0,08	1,08	55,75	0,14	0,03	0,63	0,01	0,01	0,02	2,42	0,03	<3	<2
NAM4	0,12	1,11	53,89	0,18	0,04	0,68	0,00	0,01	0,03	2,45	0,04	<3	<2
NAM9	0,04	1,25	55,01	0,14	0,07	0,69	0,01	0,03	0,01	2,29	0,04	<3	<2
ZAK17	0,08	0,96	55,80	0,18	0,05	0,72	0,00	0,01	0,00	1,62	0,03	<3	<2
ZAK18	0,08	1,17	53,72	0,25	0,04	0,77	0,01	0,00	0,01	1,64	0,04	<3	<2
ZAK19	0,00	1,04	55,12	0,21	0,05	0,84	0,01	0,00	0,02	1,28	0,04	<3	<2
ZAK20	0,00	1,02	54,66	0,25	0,04	1,00	0,01	0,04	0,01	2,51	0,03	<3	<2
ZAK22	0,12	0,95	55,36	0,26	0,02	0,60	0,01	0,00	0,00	0,79	0,03	<3	<2

Notes: In situ-produced ^{36}Cl concentrations and CRE ages of samples from the two alluvial fans, offset by the Baghan and Quchan faults. Measurements of ^{36}Cl concentrations were undertaken at the Livermore National Laboratory's CAMS. The production rates are those of Stone *et al*. (1998), corrected for elevation and latitude using the correction factors from Stone (2000). Assuming no inheritance and no erosion, ^{36}Cl cosmogenic concentrations are interpreted to give a minimum surface exposure age.

83 ± 4 kyr (Table 1, Fig. 12). This weighted-mean ^{36}Cl minimum exposure age is calculated assuming that there has been no significant erosion acting on the fan surface since its abandonment.

In the Honameh region, we dated a total of seven samples of carbonate boulders embedded in a series of displaced Q3 fan surfaces (Fig. 9). Among those samples, five were collected from two well-preserved parts of the Zakranlu alluvial fan surface (Fig. 6). The analysed samples from the Zakranlu fan yield minimum exposure ages ranging from 288 ± 34 to 448 ± 65 kyr. Among the sampled boulders, six among seven yielded minimum exposure ages ranging from 288 ± 34 to 326 ± 40 kyr. One sample is significantly older (448 ± 65 kyr). To interpret this age distribution, one can consider that the oldest sample is an outlier, indicating a previous exposure episode in the source area (inheritance). If it is so, the weighted-mean minimum ^{36}Cl exposure age of 280 ± 16 kyr is the closest evaluation of the actual abandonment age. On the other hand, since erosional processes acting on the fan surface may be responsible for exhumation of the boulders from deeper positions within the alluvial material, the oldest age (448 ± 65 kyr) may be the closest to the actual age of abandonment, which is the most conservative estimation that can be done considering the data set.

We already discussed about the regional reliability of the offset recorded by the Zakranlu alluvial fan, examining spatial consistency of the observed fault offsets recorded by other Q3 fans. To verify temporal consistency of these offsets, two other samples were collected from another Q3 fan surface approximately 9 km in the south of the Zakranlu fan (Fig. 9). Those yield minimum ^{36}Cl exposure ages of 232 ± 24 and 283 ± 32 kyr, strengthening our confidence for an isochronous abandonment age for the regional Q3 surface (Fig. 9).

In the lack of direct erosional features (i.e. even young gullies and/or differential erosion) on the sampled parts of the fan surfaces (Section 4.1.2), sensitivity of the surface exposure ages to erosion can be distinguished from the boulder age distribution patterns. In other words, soil erosion (whatever the involved mechanism) produces a distribution of apparent ages between the actual surface age and some younger age limit. The width of the distribution being proportional to the surface age and the actual age, being close to the maximum of the distribution (Zreda *et al*. 1994; Wells *et al*. 1995; Phillips *et al*. 1997).

Considering this suggestion as a guide in interpreting the age distributions observed on the offset fan surfaces, the relatively well-clustered exposure age distributions of both the Namanlu and Zakranlu boulders imply small erosion depths on the fan surfaces. In such a case, the weighted-mean boulder exposure ages of 83 ± 4 and 280 ± 16 kyr can be interpreted as the best estimate (±10 per cent; Bierman 1994) of the true abandonment age for the Namanlu and Zakranlu alluvial fan surfaces, respectively. However, the accuracy of the calculated ages depends on future improvement of ^{36}Cl production rates calibration.

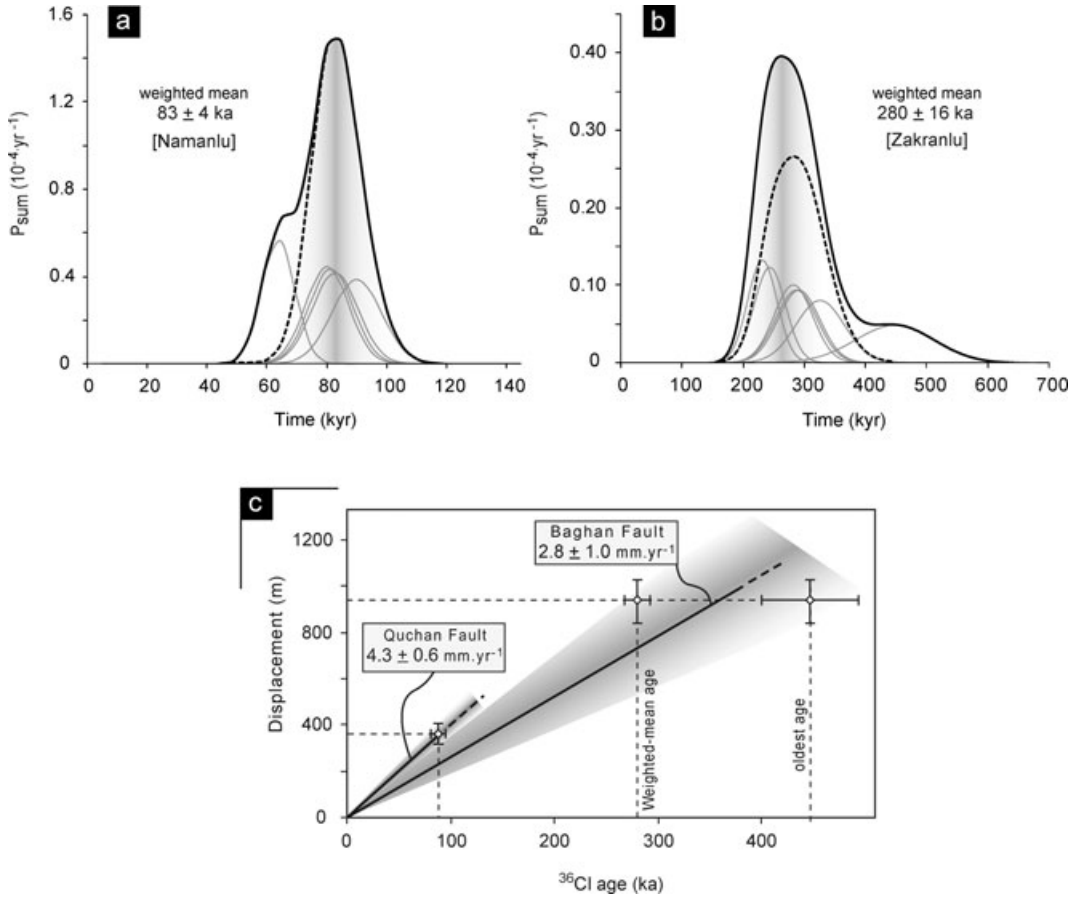

Figure 12. *In situ*-produced ^{36}Cl exposure ages of samples collected on the Namanlu (a), and Zakranlu (b) fan surfaces. Black curves are age probability sum, and grey curves represent the age probability for each individual sample. The age probability sum without outlier sample ages is presented by dotted-curves. (c) Calculated slip rates along the Quchan and Baghan faults during late Quaternary.

4.5 Long-term slip rates along the BQFS

In this study, slip rate evaluations are based on three main assumptions: (1) there has been no erosion of the sampled surfaces since their abandonment, (2) the fault slip rates remained constant since formation of the offset Quaternary markers and (3) the main traces of the Baghan and Quchan faults are assumed to have accumulated all of the horizontal strain at studied sites. Accepting these assumptions, the accuracy of our slip rates relies on the geomorphic relevance, and analytical accuracy of the obtained minimum ^{36}Cl exposure ages respect to the cumulative fault offsets.

At the Namanlu fan, the Quchan Fault runs through the fan body, and there is no evidence of post-offset deposition on any parts of the fan surface. In this case, we may conclude that the Namanlu fan surface was abandoned at minimum 83 $\pm$ 4 kyr and subsequently offset by 360 $\pm$ 50 m, yielding a maximum long-term slip rate of 4.3 $\pm$ 0.6 mm yr^{-1} for the Quchan Fault (Fig. 12).

The Zakranlu alluvial fan has been separated from its feeding watershed due to a right-lateral cumulative displacement of 940 $\pm$ 100 m along the Baghan Fault. Since the age of abandonment of the Zakranlu surface is comprised between the weighted-mean minimum ^{36}Cl exposure age of 280 $\pm$ 16 kyr and minimum exposure age of 448 $\pm$ 65 kyr (the oldest sample in the data set), yields a Late Quaternary slip rate of 2.8 $\pm$ 1.0 mm yr^{-1} for the Baghan Fault (Fig. 12).

5 DISCUSSION AND CONCLUSION

Combining high-resolution satellite images, SRTM digital topographic data and field observations, the entire fault system of Central-East Kopeh Dagh was mapped in detail (Fig. 2). Thus, we determined a precise 2-D geometry of the fault system and its individual fault segments. Analysing cumulative post-folding geological offsets (ranging from 100 m to 18 km in 337 different sites; see the Appendix) on the different fault segments, we examined the gradient changes in the distribution of strike-slip deformation over the Central-East Kopeh Dagh (Fig. 3). Regardless of possible continuous deformation (see Section 5.2), a large portion (30 $\pm$ 2 km) of the total deformation (35–40 km) is accommodated on a localized fault system (BQFS) dissecting the Central Kopeh Dagh (Fig. 3). Within this regional fault system, the Quchan and Baghan faults are the most important ones, exhibiting maximum cumulative displacements of 15.5 $\pm$ 0.5 and 9.8 $\pm$ 0.2 km, respectively (Fig. 5). The rest of this strike-slip deformation is taken up by the other strike-slip faults spread within this part of the Kopeh Dagh (Fig. 3).

Combined quantitative geomorphic and geometric analysis, as well as *in situ*-produced cosmogenic ^{36}Cl dating of two regionally distinct alluvial fan surfaces yield the first direct and well-constrained geological estimate of the Late Quaternary slip rates on the Quchan and Baghan faults, bearing the caveat in mind that the slip rates we discuss herein are maximum. The oldest

geomorphologically preserved alluvial fan shows a cumulative offset of 940 ± 100 m postdating its abandonment (between 280 ± 16 and 450 ± 65 kyr), yielding a maximum slip rate of 2.8 ± 1.0 mm yr^{-1} for the Baghan Fault. The younger alluvial fan shows a cumulative offset of 360 ± 50 m postdating its abandonment at minimum 83 ± 4 kyr, yielding a maximum slip rate of 4.3 ± 0.6 mm yr^{-1} for the Quchan Fault.

5.1 Initiation of the strike-slip motions in the Kopeh Dagh

Applying the calculated Late Quaternary slip rates to maximum post-folding cumulative geological offsets along the Baghan and Quchan faults, and assuming that the slip rates have been constant during the life of the fault; one can estimate onset of strike-slip motion on those faults. For the Quchan Fault, considering a maximum cumulative offset of 15.5 ± 0.5 km (Fig. 5) and a maximum-possible slip-rate of 4.3 ± 0.6 mm yr^{-1} yields a maximum inception age of 3.6 ± 0.6 Ma for the initiation of strike-slip motion. In the same way, the results obtained for the Baghan Fault yield a maximum inception age of 3.5 ± 1.3 Ma. It is worth noting that the slip rates have been determined independently for both faults (using deformed geomorphic markers of different ages), which strengthen the confidence one can have about the reliability of the proposed date for the beginning of the strike-slip motion along the Baghan and Quchan faults.

From the local geomorphic point of view, our detailed mapping provides evidences that both fold axes and Plio-Quaternary alluvial plains are offset about the same amount of right-lateral cumulative displacements along the Baghan and Quchan faults (Fig. 5). This strongly supports the idea that the strike-slip motion should be started no earlier than the Pliocene. From the regional plate kinematics perspective, our estimated age for inception of strike-slip motions on both faults is in good agreement with (1) the stratigraphic-derived value of 4 Ma for the beginning of strike-slip faulting in the Kopeh Dagh (Afshar Harb 1979), (2) the timing of widespread reorganization of tectonic deformation in the Middle East at roughly 5 Ma (Hempton 1987; Westaway 1994; Axen *et al*. 2001), which is emphasized by the present-day distribution of active faulting within the Arabia–Eurasia collision margin at 3–5 Ma (Bozkurt 2001; Koçyigit *et al*. 2001; Talebian & Jackson 2002; Allen *et al*. 2004; Regard *et al*. 2004; Walker & Jackson 2004; Authemayou *et al*. 2006; Copley & Jackson 2006), and a possible change in the rotation of the plates bordering the Dead Sea fault in the early to late Pliocene (Ron *et al*. 1984; Livnat *et al*. 1987).

The time and duration of tectonic reorganization in the Arabia–Eurasia collision zone are suggested to be diachronous (i.e. Allen *et al*. 2004), but the apparent age differences might also arise either from age uncertainties due to the lack of direct dating of corresponding tectonic events, or because of confusing and ambiguous cause-and-effect relationships between the events, that is, the relationships between the South Caspian Basin subsidence/subduction and rapid exhumation of the west-central Alborz (see Devlin *et al*. 1999; Axen *et al*. 2001; Allen *et al*. 2002; Jackson *et al*. 2002; Allen *et al*. 2004). In the present study, different geomorphic and geological arguments accompanied with *in situ*-produced cosmogenic ^{36}Cl dating allow us to constrain the age of this tectonic reorganization in the Central Eastern Kopeh Dagh at ∼4°Ma.

5.2 Integrating our data-derived results within pre-existing models

The main results of our study are (1) the well-constrained Late Quaternary slip rates on the Quchan and Baghan faults and (2) the initiation of strike-slip motion along these faults that can be considered as the time of a major tectonic reorganization in the Central Eastern Kopeh Dagh. The minimum bound of our slip rate bracketing is close to the revised average geological slip rate of ∼6 mm yr^{-1} estimated for the Quchan and Baghan faults (Afshar Harb 1979), assuming that the post-folding total displacement along these faults (∼25 km, Afshar Harb *et al*. 1987) occurred over the last 4 Ma. Conversely, our results are not in agreement with the model-derived estimate of Hollingsworth *et al*. (2006) that proposes the respective slip rates of ∼1.5 and ∼1 mm yr^{-1} for the Quchan and Baghan faults during the last 10 Ma.

To calculate these slip rates, Hollingsworth *et al*. (2006) assumed that the maximum offsets achieved in 10 Ma, a time span calculated dividing 70 km of total deformation (10 km for N–S shortening before the onset of strike-slip faulting plus 60 km for post-folding N–S motion) by the present-day GPS-derived rate of 7 mm yr^{-1} for northward motion of central Iran with respect to Eurasia. Accepting the proposed value of 10 Ma for the initiation of strike-slip faulting (Hollingsworth *et al*. 2006), it comes into conflict with its pre-strike-slip nature, that is, 10 km of N–S shortening before the onset of strike-slip faulting. Therefore, this overestimated age for the initiation of strike-slip faulting (10 Ma) yields at best underestimated fault slip rates.

The model proposed by Hollingsworth *et al*. (2006) is based on anticlockwise rigid block rotation around a vertical axis, allowing across-strike shortening and along-strike elongation in the Kopeh Dagh Mountains. However, the application of this model need (1) that all the involved faults, which define lateral limits of the rotating blocks (i.e. the Baghan, Quchan and Dorbadam faults), should be cutting across the deforming zone, (2) that blocks with the same width should represent the same rotation angle, and consequently the same apparent strike-slip displacement and (3) that the displacement gradient has to be constant along length of the faults regardless the distance from fault terminations. To the contrary, the data set, provided in this study, indicates that the strike-slip brittle deformation is heterogeneously distributed on several fault segments within the Central-Eastern Kopeh Dagh (Fig. 3), and not homogenously localized on three faults cutting across the range, which strongly favours a simple strike-slip faulting mechanism that moves the Western Kopeh Dagh northwards relative to the east.

5.3 Distribution of slip rates in the Kopeh Dagh

Based on the distribution of cumulative displacements along the different fault segments mapped within the BQFS (see Section 3.2), one can infer the regional distribution of fault slip rates. To regionally propagate the results obtained for the Quchan and Baghan faults, it must be assumed that the initiation of all strike-slip faults in the Kopeh Dagh is contemporaneous (at ∼4 Ma). If this assumption is correct, then differences in measured cumulative geological offsets should reflect long-term fault slip rate differences on individual fault segments. Fig. 3 shows the regional distribution of cumulative displacements and consequent maximum long-term slip rates derived from the above assumption. This figure illustrates how the deformation is mainly localized along the BQFS in which, the Baghan and Quchan faults have the highest slip rates. At the regional scale, one can also budget the sum of total cumulative offsets across the Kopeh Dagh at about 35–40 km. In fact, this sum is accommodated along at least eleven distinct fault segments, making it different from the proposed value by Hollingsworth *et al* (2006) for only three faults. We note that, because slip rates for the Baghan and Quchan faults are maximum rates, it is more reliable

considering the upper bound of the inception age estimate (3.5–5.1 Ma) to calculate the total slip rate of strike-slip faulting in the Kopeh Dagh. Applying the deduced time span of 4.3 ± 0.8 Myr for accumulation of the offsets, this bracketed value implies a total slip rate of about 9 ± 2 mm yr^{-1} (Fig. 3) to be distributed over all the right-lateral strike-slip faults in the Central Eastern Kopeh Dagh. Consequently, this total slip rate has to be accommodated on the northeastern boundary of the Arabia–Eurasia collision zone. According to these results, in northeast Iran, a large part of the northward motion between central Iran and Eurasia (30 ± 2 km) seems to be accommodated along the BQFS as strike-slip deformation, which indicates that the BQFS can be considered as an intercontinental boundary between Iranian microplate and Eurasia, accommodating about 80 per cent of northward motion of central Iran with respect to Eurasia.

It is noteworthy that no evidence of deep-seated active thrust faulting is observed in the central part of the Kopeh Dagh. Moreover, the internal deformation of the blocks between strike-slip faults seems to be low, as evidenced by non-deformed linear markers such as anticline axes and ridge crests (Fig. 5). In addition, thanks to high resolution satellite imagery and well-stratified formations, geological cumulative offsets from 100 m up to 18 km are taken into account in our measurements, which make our estimate reliable with respect to the total geological deformation in this part of the Kopeh Dagh. Therefore, the total slip rate of 9 ± 2 mm yr^{-1} is comparable with the maximum bound of geodetic/geodynamic-derived rate of 8–10 mm yr^{-1} proposed for the northward motion between central Iran and Eurasia (Vernant *et al*. 2004; Reilinger *et al*. 2006), and close to the total GPS rate of 9 ± 2 mm yr^{-1} for strike-slip motion in the Kopeh Dagh (Tavakoli 2007). Though, long-term geological slip rates do not necessarily need to be identical to such short-term rates integrated over the last several years.

Resolving the total strike-slip displacement value of 35–40 km on a regional average structural orientation representative of the BQFS (azimuth: N28°W, dip: 75°NE, rake: 10°) deduced from direct field observations and satellite image mapping, total ∼34 km northward and ∼16 km westward displacements can be derived for Central and Western Kopeh Dagh with respect to Eurasia. If one accepts the calculated values as representative for the total deformation of this part of the Kopeh Dagh, these imply an averaged northward slip rate of roughly 8 mm yr^{-1}, and an averaged westward slip rate of about 4 mm yr^{-1}. Recent GPS measurements in the Kopeh Dagh (Tavakoli 2007) evaluated a total northward motion rate of about 8 ± 2 mm yr^{-1} at the longitude of ∼56°E, and a rate of 5 ± 2 mm yr^{-1} between the Western and Eastern Kopeh Dagh toward the South Caspian Basin, accommodated by right-lateral slip on the MKDF and by left-lateral slip on the Shahrud fault system (at the southern boundary of the Western Kopeh Dagh, west of ∼56°E). This consistency between our geological and geomorphic estimates and GPS rates indicates that regardless some probable errors in both measurements, they may have be representative of the total deformation in the Central-Eastern Kopeh Dagh since emplacement of the present-day tectonic configuration at ∼4 Ma.

ACKNOWLEDGMENTS

This work was funded by the INSU-CNRS (France) and the International Institute of Earthquake Engineering and Seismology (IIEES, Iran), supervised by D. Hatzfeld and M.G. Ashtiani. Funding was provided by the Dyeti and PNRN programs (INSU-CNRS) and ACI FNS program (French Ministry of Research), within the above-mentioned co-operative agreement. SPOT images were provided thanks to the ISIS program (©CNES 2004 to 2007, distribution SPOT images S.A.). E.S. benefits of a Foreign Affair Ministry (Ministère des Affaires Etrangères) grant through French Embassy in Iran, and a complement support through the 'Cotutelle de thèse' program (ACI du Ministère des Affaires Etrangères). We thank V. Grimault, Ch. Duhamel and the staff of the SCAC of the French Embassy in Tehran, for their support. We greatly acknowledge R. Finkel at CAMS-LLNL (Lawrence Livermore National Laboratory), who performed the ^{36}Cl measurements. We are grateful to two anonymous reviewers for constructive reviews. We thank D. Bourlès, R. Braucher, D. Hatzfeld, I. Schimmelpfennig and M. Djamali for fruitful discussions and help during the course of this work. The General governments of Khorassan-e Razavi and Shomali provinces have efficiently helped us during 3 yr. Mohsen Zolfaqary with his careful driving provided excellent assistance in the field. We thank J. Crider for comments and English language corrections. A. Afshar Harb provided the basic geological knowledge of the Kopeh Dagh through his pioneering work in NE Iran: this paper is dedicated to his memory.

REFERENCES

Afshar Harb, A., 1979. The stratigraphy, tectonics and petroleum geology of the Kopet Dagh region, northeastern Iran, *PhD thesis*. Petroleum Geology Section, Royal School of Mines, Imperial College of Science and Technology, London.

Afshar Harb, A., 1982. Geological quadrangle map of Iran no. K3 (Darreh Gaz sheet), scale 1:250 000, Geological Survey of Iran.

Afshar Harb, A., Soheili, B.M. & Valeh, C.N., 1980. Geological quadrangle map of Iran no. I3 (Kuh-e Kurkhud sheet), scale 1:250 000, Geological Survey of Iran.

Afshar Harb, A., Bolourchi, M. & Mehr Parto, M., 1987. Geological quadrangle map of Iran no. J5 (Bojnurd sheet), scale 1:250 000, Geological Survey of Iran.

Allen, M.B., Jones, S., Ismail-Zadeh, A., Simmons, M. & Anderson, L., 2002. Onset of subduction as the cause of rapid Pliocene-Quaternary subsidence in the South Caspian Basin, *Geology,* **30**(9), 775–778, doi:10.1130/0091–7613(2002)030<0775.

Allen, M., Jackson, J. & Walker, R., 2004. Late Cenozoic reorganization of the Arabia-Eurasia collision and the comparison of short-term and long-term deformation rates, *Tectonics,* **23,** TC2008, doi:10.1029/2003TC00153.

Allen, M.B., Blanc, E.J.-P., Walker, R., Jackson, J., Talebian, M. & Ghassemi, M.R., 2006. Contrasting styles of convergence in the Arabia-Eurasia collision: why escape tectonics does not occur in Iran, in *Postcollisional Tectonics and Magmatism in the Mediterranean Region and Asia,* Vol. 409, pp. 579–589, eds Dilek, Y. & Pavlides, S., Geol. Soc. Am. Special Paper, doi:10.1130/2006.2409(26).

Ambraseys, N. & Melville, C., 1982. *A History of Persian Earthquakes,* Cambridge University Press, Cambridge, UK.

Amurskiy, G.I., 1971. The deep structure of the Kopetdagh, *Geotectonics,* **1,** 34–40 (Engl. Transl.).

Authemayou, C., Bellier, O., Chardon, D., Malekzade, Z. & Abbassi, M., 2005. Role of the Kazerun fault system in active deformation of the Zagros fold and-thrust belt (Iran), *C. R. Geoscience,* **337,** 539–545.

Authemayou, C., Chardon, D., Bellier, O., Malekzade, Z., Shabanian, E. & Abbassi, M., 2006. Late Cenozoic partitioning of oblique plate convergence in the Zagros fold-and-thrust belt (Iran), *Tectonics,* **25,** TC3002, doi:10.1029/2005TCOO1860.

Axen, G.J., Lam, P.S., Grove, M., Stockli, D.F. & Hassanzadeh, J., 2001. Exhumation of the west-central Alborz Mountains, Iran, Caspian subsidence, and collision-related tectonics, *Geology,* **29**(6), 559–562.

Bayer, R. *et al*., 2006. Active deformation in Zagros-Makran transition zone inferred from GPS measurements, *Geophys. J. Int.,* **165**(1), 373–381, doi:10.1111/j.1365-246X.2006.02879.x.

Berberian, M. & Yeats, R., 1999. Patterns of historical earthquake rupture in the Iranian Plateau, *Bull. seism. Soc. Am.,* **89,** 120–139.

Berberian, M. & Yeats, R., 2001. Contribution of archaeological data to studies of earthquake history in the Iranian Plateau, *J. Strct. Geol.,* **23,** 563–584.

Bierman, P.R., 1994. Using *in situ* produced cosmogenic isotopes to estimate rates of landscape evolution: a review from the geomorphic perspective, *J. geophys. Res.,* **99**(B7), 13 885–13 896.

Bierman, P.R., Gillespie, A.R., Caffee, M.W. & Elmore, D., 1995. Estimating erosion rates and exposure ages with ^{36}Cl produced by neutron activation, *Geochim. Cosmochim. Acta,* **59,** 3779–3798.

Bozkurt, E., 2001. Neotectonics of Turkey—a synthesis, *Geodin. Acta,* **14**(1), 3–30, doi:10.1016/S0985-3111(01)01066-X.

Copley, A. & Jackson, J., 2006. Active tectonics of the Turkish-Iranian Plateau, *Tectonics,* **25,** TC6006, doi:10.1029/2005TC001906.

Daëron, M., Benedetti, L., Tapponnier, P., Sursock, A. & Finkel, R.C., 2004. Constraints on the post ∼25-ka slip rate of the Yammoûneh fault (Lebanon) using in situ cosmogenic ^{36}Cl dating of offset limestone-clast fans, *Earth planet. Sci. Lett.,* **227,** 105–119.

Deino, A. and Potts, R., 1992. Age-probability spectra from examination of single-crystal ^{40}Ar/^{39}Ar dating results: examples from Olorgesailie, Southern Kenya Rift, *Quater. Int.,* **13/14,** 47–53.

Devlin, W., Cogswell, J., Gaskins, G., Isaksen, G., Pitcher, D., Puls, D., Stanley, K. & Wall, G., 1999. South Caspian Basin: Young, cool, and full of promise, *GSA Today,* **9**(7), 1–9.

Dixon, T.H, Norabuena, E. & Hotaling, L., 2003. Paleoseismology and Global Positioning System: earthquake cycle effects and geodetic versus geologic fault slip rates in the Eastern California shear zone, *Geology,* **31,** 55–58.

Friedrich, A.M., Wernicke, B.P., Niemi, N.A., Bennett, R.A. & Davis J.L., 2003. Comparison of geodetic and geologic data from the Wasatch region, Utah, and implications for the spectral character of Earth deformation at periods of 10 to 10 million years, *J. geophys. Res.,* **108**(B4), 2199, doi:10.1029/2001JB000682.

Gosse, J.C. & Phillips, F.M., 2001. Terrestrial in situ cosmogenic nuclides: theory and application, *Quater. Sci. Rev.,* **20,** 1475–1560.

Hempton, M R., 1987. Constraints on Arabian plate motion and extensional history of the Red Sea, *Tectonics,* **6**(6), 687–705, doi:10.1029/TC006i006p00687.

Hollingsworth, J., Jackson, J., Walker, R., Gheitanchi, M.R. & Bolourchi, M.J., 2006. Strike-slip faulting, rotation and along-strike elongation in the Kopeh Dagh Mountains, NE Iran, *Geophys. J. Int.,* **166,** 1161–1177, doi:10.1111/j.1365-246X.2006.02983.x.

Hollingsworth, J., Jackson, J., Alarcón, J.E., Bommer, J.J. & Bolourchi, M.J., 2007. The 4th February 1997 Bojnurd (Garmkhan) earthquake in NE Iran: field, teleseismic, and strong-motion evidence for rupture directivity effects on a strike-slip fault, *J. Earthq. Eng.,* **11,** 193–214.

Huber, H., 1977. *Geological Map of Iran Sheet no. 3, North East Iran, Scale: 1:1 000 000,* National Iranian Oil Company.

Jackson, J. & McKenzie, D., 1984. Active tectonics of the Alpine-Himalayan Belt between western Turkey and Pakistan, *Geophys. J. R. astr. Soc.,* **77**(1), 185–264.

Jackson, J., Priestley, K., Allen, M. & Berberian, M., 2002. Active tectonics of the South Caspian Basin, *Geophys. J. Int.,* **148,** 214–245.

Keller, E.A., Seaver, D.B., Laduzinsky, D.L., Johnson, D.L. & Ku, T.L., 2000. Tectonic geomorphology of active folding over buried reverse faults: San Emigdio Mountain front, southern San Joaquin Valley, California, *Geol. Soc. Am. Bull.,* **112**(1), 86–97.

Koçyigit, A., Yilmaz, A., Adamia, S. & Kuloshvili, S., 2001. Neotectonics of East Anatolian Plateau (Turkey) and Lesser Caucasus: implication for transition from thrusting to strike-slip faulting, *Geodin. Acta,* **14**(1), 177–195, doi:10.1016/S0985-3111(00)01064-0.

Livnat, A., Lifshitz, A. & Flexer, A., 1987. The tectonic style of the southern Arava Rift margins, Israel: alternating stress fields in wrench-rifting processes, *Tectonophysics,* **141**(1–3), 151–168, doi:10.1016/0040-1951(87)90182-X.

Lowell, T.V., 1995. The application of radiocarbon age estimates to the dating of glacial sequences: an example from the Miami sublobe, Ohio, USA, *Quarter. Sci. Rev.,* **14,** 85– 99.

Lyberis, N. & Manby, G., 1999. Oblique to orthogonal convergence across the Turan block in the post-Miocene, *Am. Assoc. Petrol. Geol. Bull.,* **83**(7), 1135–1160.

Lyberis, N., Manby, G., Poli, J.T., Kalugin, V., Yousouphocaev, H. & Ashirov, T., 1998. Post-Triassic evolution of the southern margin of the Turan plate, *C. R. Acad. Sci.,* **326,** 137–143.

Maggi, M., Jackson, J., McKenzie, D. & Priestley, K., 2000. Earthquake focal depths, effective elastic thickness, and the strength of the continental lithosphere, *Geology,* **28**(6), 495–498.

Masson, F., Djamour, Y., Vangorp, S., Chéry, J., Tavakoli, F., Tatar M. & Nankali, H., 2006. Extension in NW Iran inferred from GPS enlightens the behavior of the south Caspian basin, *Earth planet. Sci. Lett.,* **252,** 180–188.

Masson, F., Anvari, M., Djamour, Y., Walpersdorf, A., Tavakoli, F., Daignières, M., Nankali, H. & Van Gorp, S., 2007. Large-scale velocity field and strain tensor in Iran inferred from GPS measurements: new insight for the present-day deformation pattern within NE Iran, *Geophys. J. Int.,* **170,** 436–440, doi:10.1111/j.1365-246X.2007.03477.x.

McClusky, S., Reilinger, R., Mahmoud, S., Ben Sari, D. & Tealeb, A., 2003. GPS constraints on Africa (Nubia) and Arabia plate motions, *Geophys. J. Int.,* **155**(1), 126–138, doi:10.1046/j.1365-246X.2003.02023.x.

McDonald, E.V., 1994. The relative influence of climatic change, desert dust, and lithological control on soil-geomorphic processes and hydrology of calcic soils formed on Quaternary alluvial-fan deposits in the Mojave Desert, California, *PhD thesis*. Univ. of New Mexico, Albuquerque.

McFadden, L.D., McDonald, E.V., Wells, S.G., Anderson, K., Quade, J. & Forman, S.L., 1998. The vesicular layer and carbonate collars of desert soils and pavements: formation, age and relation to climate change, *Geomorphology,* **24,** 101–145.

McKenzie, D.P., 1972. Active tectonics of the Mediterranean region, *Geophys. J. Int.,* **30**(2), 109–185, doi:10.1111/j.1365-246X.1972.tb02351.x.

Phillips, F.M., Zreda, M.G., Flinsch, M.R., Elmore, D. & Sharma, P., 1996. A reevaluation of cosmogenic ^{36}Cl production rates in terrestrial rocks, *Geophys. Res. Lett.,* **23,** 949–952.

Phillips, F.M., Zreda, M.G., Gosse, J.C., Klein, J., Evenson, E.B., Hall, R.D., Chadwick, O.A. & Sharma, P., 1997. Cosmogenic ^{36}Cl and ^{10}Be ages of Quaternary glacial and fluvial deposits of the Wind River Range, Wyoming, *Geol. Soc. Am. Bull.,* **109**(11), 1453–1463.

Regard, V., Bellier, O., Thomas, J.-C., Abbassi, M.R., Mercier, J.L., Shabanian, E., Feghhi, K. & Soleymani, S., 2004. Accommodation of Arabia-Eurasia convergence in the Zagros-Makran transfer zone, SE Iran: a transition between collision and subduction through a young deforming system, *Tectonics,* **23,** TC4007, doi:10.1029/2003TC001599.

Regard, V. *et al*., 2005. Cumulative right-lateral fault slip rate across the Zagros–Makran transfer zone: role of the Minab–Zendan fault system in accommodating Arabia–Eurasia convergence in southeast Iran, *Geophys. J. Int.,* **162,** 177–203, doi:10.1111/j.1365-246X.2005.02558.x.

Regard, V. *et al*., 2006. ^{10}Be dating of alluvial deposits from Southeastern Iran (the Hormoz Strait area), *Palaeogeogr., Palaeoclimat., Palaeoecol.,* **242**(1–2), 36–53, doi:10.1016/j.palaeo.2006.05.012.

Reilinger, R. *et al*., 2006. GPS constraints on continental deformation in the Africa-Arabia-Eurasia continental collision zone and implications for the dynamics of plate interactions, *J. geophys. Res.,* **111,** B05411, doi:10.1029/2005JB004051.

Ritz, J.F., Brown, E.T., Bourlès, D., Philip, H., Schlupp, A., Raisbeck, G.M., Yiou, F. & Enkhtuvshin, B., 1995. Slip rates along active faults estimated with cosmic-ray–exposure dates: application to the Bogd fault, Gobi-Altaï, *Mongolia, Geology,* **23**(11), 1019–1022.

Ritz, J.-F., Nazari, H., Ghassemi, A., Salamati, R., Shafei, A., Solaymani, S. & Vernant, P., 2006. Active transtension inside central Alborz: a new insight into northern Iran–southern Caspian geodynamics, *Geology,* **34**(6), 477–480, doi:10.1130/G22319.1.

Ron, H., Freund, R., Garfunkel, Z. & Nur, A., 1984. Block-rotation by strike–slip faulting: structural and paleomagnetic evidence, *J. geophys. Res.,* **89**(B7), 6256–6270.

Schimmelpfennig, I., Benedetti, L., Finkel, R., Pik, R., Blard, P.H., Bourlès, D., Burnard, P. & Williams, A., 2009. Sources of in-situ 36Cl in basaltic rocks. Implications for calibration of production rates, *Quarter. Geochronol.,* submitted.

Sella, G.F., Dixon, T.H. & Mao, A., 2002. REVEL: a model for recent plate velocities from space Geodesy, *J. geophys. Res.,* **107**(B4), 2081, doi:10.1029/2000JB000033.

Stöcklin, J., 1968. Structural history and tectonics of Iran: a review, *Am. Assoc. Petrol. Geol. Bull.,* **52**(7), 1229–1258.

Stone, J.O.H., 2000. Air pressure and cosmogenic isotope production, *J. geophys. Res.,* **105**(B10), 23 753–23 759.

Stone, J.O.H., Allan, G.L., Fifield, L.K. & Cresswell, R.G., 1996. Cosmogenic chlorine-36 from calcium spallation, *Geochim. Cosmochim. Acta,* **60**(4), 679–692.

Stone, J.O.H., Evans, J.M., Fifield, L.K., Allan, G.L. & Cresswell, R.G., 1998. Cosmogenic chlorine-36 production in calcite by muons, *Geochim. Cosmochim. Acta,* **62**(3), 433–454.

Talebian, M. & Jackson, J., 2002. Offset on the Main Recent Fault of NW Iran and implications for the late Cenozoic tectonics of the Arabia–Eurasia collision zone, *Geophys. J. Int.,* **150,** 422–439.

Talebian, M. & Jackson, J., 2004. A reappraisal of earthquake focal mechanisms and active shortening in the Zagros mountains of Iran, *Geophys. J. Int.,* **156**(3), 506–526.

Tapponnier, P., Frederick, J.R., Van Der Woerd, J., Mériaux, A.S. & Lasserre, C., 2001. Long-term slip rates and characteristic slip: keys to active fault behaviour and earthquake hazard, *C. R. Acad. Sci. Ser. II,* **333**(9), 483–494.

Tavakoli, F., 2007. Present-day kinematics of the Zagros and east of Iran faults, *PhD thesis*. University of Joseph Fourier, Grenoble.

Taylor, J.R., 1997. *An Introduction to Error Analysis, The Study of Uncertainties in Physical Measurements,* 2nd edn, University Science Books, Sausalito, CA.

Tchalenko, J.S., 1975. Seismicity and structure of the Kopet Dagh (Iran, USSR), *Phil. Trans. R. Soc. Lond., Series A,* **278**(1275), 1–28.

Tchalenko, J.S., Braud, J. & Berberian, M., 1974. Discovery of three earthquake faults in Iran, *Nature,* **248,** 661–663.

Trifonov, V., 1978. Late Quaternary tectonic movements of western and central Asia, *Geol. Soc. Am. Bull.,* **89,** 1059–1072.

Vernant, P. *et al*., 2004. Present-day crustal deformation and plate kinematics in the Middle East constrained by GPS measurements in Iran and northern Oman, *Geophys. J. Int.,* **157**(1), 381–398, doi:10.1111/j.1365-246X.2004.02222.x.

Walker, R. & Jackson, J., 2004. Active tectonics and Late Cenozoic strain distribution in central and eastern Iran, *Tectonics,* **23,** TC5010, doi:10.1029/2003TC001529.

Walpersdorf, A. *et al*., 2006. Difference in the GPS deformation pattern of North and Central Zagros (Iran), *Geophys. J. Int.,* **167**(3), 1077–1088, doi:10.1111/j.1365-246X.2006.03147.x.

Wells, S.G., McFadden, L.D., Dohrenwend, J.C., Turrin, B.D. & Mahrer, K.D., 1985. Late Cenozoic landscape evolution of lava flow surfaces of the Cima volcanic field, Mojave Desert, California, *Geol. Soc. Am. Bull.,* **96,** 1518–1529.

Wells, S.G., McFadden, L.D. & Dohrenwend, J.C., 1987. Influence of Late Quaternary climatic changes on geomorphic and pedogenic processes on a desert piedmont, eastern Mojave Desert, California, *Quarter. Res.,* **27,** 130–146.

Wells, S.G., McFadden, L.D., Poths, J. & Olinger, C.T., 1995. Cosmogenic ^{3}He exposure dating of stone pavements: implications for landscape evolution in deserts, *Geology,* **23,** 613–616.

Westaway, R., 1994. Present-day kinematics of the Middle East and eastern Mediterranean, *J. geophys. Res.,* **99**(B6), 12 071–12 090.

Yamini-Fard, F., Hatzfeld, D., Farahbod, A.M., Paul, A. & Mokhtari, M., 2007. The diffuse transition between the Zagros continental collision and the Makran oceanic subduction (Iran): microearthquake seismicity and crustal structure, *Geophys. J. Int.,* **170**(1), 182–194.

Zreda, M.G., Phillips, F.M., & Elmore, D., 1994. Cosmogenic ^{36}Cl accumulation in unstable landforms, 2. Simulations and measurements on eroding moraines, *Water Resour. Res.,* **30,** 3127–3136.

APPENDIX

Detailed characteristics of the post-folding cumulative fault displacements (presented in Fig. 3), measured along the strike-slip faults within the Central-Eastern Kopeh Dagh; the point locations are described in latitude/longitude (WGS84 projection system), extracted from SPOT5 or LANDSAT ETM+ satellite images.

Longitude (°E)	Latitude (°N)	Offset (m)	Slip rate (mm yr^{-1})
59,7469	37,7112	0	0,00
56,859	37,9679	170	0,05
57,2495	37,8339	180	0,05
57,7218	37,6526	180	0,05
57,0518	37,9166	200	0,06
57,2	37,9759	200	0,06
58,1261	37,8688	200	0,06
58,2183	37,555	200	0,06
57,2351	37,8987	210	0,06
57,7116	37,6577	210	0,06
56,9046	37,9598	220	0,06
57,2402	37,8743	220	0,06
57,2842	37,8366	230	0,07
57,0292	37,9172	240	0,07
57,0367	37,91	240	0,07
56,6556	37,354	250	0,07
56,8678	38,3948	250	0,07
56,8788	38,3995	250	0,07
57,02	37,9261	270	0,08
57,2702	37,8263	270	0,08
57,3186	37,9188	280	0,08
56,8957	38,4016	300	0,09
57,275	37,8484	300	0,09
57,3822	37,9099	300	0,09
57,7361	37,6502	300	0,09
57,783	37,3149	300	0,09
58,8768	37,2923	300	0,09
59,0249	36,8677	300	0,09
57,3041	37,8185	310	0,09
56,8974	37,9476	320	0,09
56,9259	37,955	330	0,09
59,0126	36,8532	330	0,09
56,6163	37,3439	350	0,10
56,6362	37,3489	350	0,10
56,9326	37,6312	350	0,10
57,0964	37,7527	350	0,10
57,2588	37,8434	350	0,10
57,1757	37,9854	370	0,11
56,9007	38,004	400	0,11
57,1146	37,7694	400	0,11
58,9811	36,9059	400	0,11
59,0502	36,9379	400	0,11
56,9327	37,9366	410	0,12
57,7541	37,6479	410	0,12
56,9567	37,9447	420	0,12
56,9123	37,9815	450	0,13
57,6751	37,3004	450	0,13
58,468	37,3763	450	0,13
58,9897	36,8849	450	0,13
59,5757	37,1655	450	0,13
57,0797	37,7612	470	0,13
56,9416	38,0297	480	0,14
57,0883	38,1237	480	0,14
57,1349	38,071	480	0,14
59,0064	36,8405	490	0,14
56,3621	38,0975	500	0,14

Longitude (°E)	Latitude (°N)	Offset (m)	Slip rate (mm yr^{-1})
56,9364	38,0055	500	0,14
56,9751	38,0219	500	0,14
57,0082	38,1926	500	0,14
57,0131	38,0253	500	0,14
57,0677	38,0892	500	0,14
57,1219	37,994	500	0,14
58,282	37,7376	500	0,14
58,4368	37,4722	500	0,14
59,0987	36,8349	500	0,14
59,1071	36,8214	500	0,14
58,6644	37,5591	520	0,15
59,087	36,8564	520	0,15
56,266	38,1119	530	0,15
59,5063	37,1946	540	0,15
56,2429	38,0975	550	0,16
56,6233	37,199	550	0,16
56,8831	37,9508	550	0,16
56,2952	38,1293	560	0,16
56,9091	37,9355	560	0,16
57,0086	37,9295	580	0,17
59,4785	37,2111	580	0,17
59,0308	36,9783	590	0,17
56,397	38,1226	600	0,17
56,6033	37,1993	600	0,17
56,7998	37,8886	600	0,17
57,0533	38,0081	600	0,17
57,1032	37,9993	600	0,17
58,6915	37,5545	600	0,17
59,0816	36,8724	600	0,17
59,3378	37,271	600	0,17
59,4008	37,2482	600	0,17
56,8747	37,965	610	0,17
58,956	36,8909	610	0,17
58,2928	37,7171	620	0,18
57,1814	38,0811	630	0,18
57,2202	38,0345	630	0,18
57,2667	37,9838	630	0,18
57,2926	37,9149	630	0,18
57,5102	37,4402	630	0,18
57,2475	37,8927	640	0,18
57,6444	36,9911	640	0,18
57,1677	37,9979	650	0,19
57,6338	37,0003	650	0,19
57,6684	36,973	660	0,19
57,6902	36,9525	660	0,19
56,953	37,9319	670	0,19
56,8197	38,0489	680	0,19
58,2599	37,5359	680	0,19
56,7872	37,6358	700	0,20
56,8255	37,9892	700	0,20
56,8339	37,6665	700	0,20
56,9743	37,9392	700	0,20
57,3604	37,9368	700	0,20
58,0082	38,0359	700	0,20
58,3082	37,683	700	0,20
56,8611	37,9157	720	0,21
58,0061	38,0111	720	0,21
57,6118	37,4384	730	0,21
57,4802	37,4264	740	0,21
56,826	38,0248	750	0,21
56,9024	38,054	750	0,21
57,1366	37,7476	750	0,21
57,2419	37,9348	750	0,21
57,5745	37,1544	750	0,21
57,8455	36,9261	750	0,21
58,2283	37,5579	750	0,21
58,2445	37,533	750	0,21
58,9557	36,9671	750	0,21
58,143	37,9514	760	0,22
58,1689	37,9109	760	0,22
58,1689	37,8724	760	0,22
58,1973	37,8278	760	0,22
58,2387	37,769	760	0,22
58,2593	37,7082	760	0,22
56,8468	37,9565	780	0,22
57,0276	37,8117	780	0,22
57,0524	37,8173	780	0,22
56,7746	37,975	790	0,23
57,0175	37,9895	790	0,23
57,6828	37,5949	790	0,23
57,9425	37,3667	800	0,23
58,4119	37,398	800	0,23
58,4354	37,3524	800	0,23
56,7555	37,6489	810	0,23
56,8664	38,0045	830	0,24
57,5011	37,7508	830	0,24
57,0712	37,9118	840	0,24
57,6239	37,7931	840	0,24
56,9824	37,5622	870	0,25
56,8838	37,857	900	0,26
58,2205	37,6874	900	0,26
58,9181	37,3093	900	0,26
58,1599	37,8314	930	0,27
58,6565	37,2585	930	0,27
56,2769	38,1607	950	0,27
57,0249	37,9507	950	0,27
57,674	37,6838	950	0,27
58,187	37,7832	950	0,27
58,9535	37,2398	950	0,27
56,8436	37,8705	970	0,28
56,5572	38,3961	980	0,28
56,9955	37,9199	980	0,28
57,0075	38,0148	1000	0,29
57,0208	37,9755	1000	0,29
57,0873	37,5895	1000	0,29
57,1116	38,1379	1000	0,29
57,14	38,0933	1000	0,29
57,184	38,0406	1000	0,29
57,2228	37,9778	1000	0,29
57,5335	37,7698	1000	0,29
57,8897	37,6738	1000	0,29
57,9233	37,6211	1000	0,29
57,9517	37,5643	1000	0,29
58,0207	37,1876	1000	0,29
58,0938	37,1984	1000	0,29
58,1393	37,2051	1000	0,29
59,064	37,2768	1000	0,29
57,6487	37,5543	1010	0,29
57,0391	37,7165	1050	0,30
57,5634	37,7915	1060	0,30
57,9397	36,9727	1100	0,31
58,2788	37,6079	1100	0,31
58,5308	37,7386	1100	0,31
58,554	37,7123	1100	0,31
58,5928	37,6778	1100	0,31
58,6264	37,6494	1100	0,31
58,4236	37,418	1150	0,33
57,304	37,6574	1200	0,34
58,3938	37,461	1200	0,34
59,3502	36,9703	1200	0,34

Longitude (°E)	Latitude (°N)	Offset (m)	Slip rate (mm yr^{-1})
57,689	37,542	1240	0,35
58,7419	37,0919	1250	0,36
59,3276	37,0047	1250	0,36
59,3402	36,9893	1250	0,36
56,4527	37,4096	1300	0,37
56,807	37,2574	1300	0,37
57,059	37,5805	1300	0,37
57,525	37,7437	1300	0,37
58,2195	37,0067	1300	0,37
58,251	37,0065	1300	0,37
58,3834	37,3819	1300	0,37
59,4385	36,8543	1300	0,37
58,4222	37,3171	1350	0,39
58,4274	37,2583	1350	0,39
57,3081	37,8541	1370	0,39
57,3184	37,8156	1370	0,39
57,3236	37,765	1370	0,39
56,5804	37,6839	1400	0,40
58,3989	37,8075	1400	0,40
58,4429	37,7528	1400	0,40
58,4946	37,7001	1400	0,40
58,5256	37,6576	1400	0,40
57,4479	37,1912	1500	0,43
57,5636	37,563	1500	0,43
58,289	37,6161	1500	0,43
58,5216	36,8805	1500	0,43
59,1905	37,191	1500	0,43
58,5251	36,9063	1560	0,45
58,5157	36,8421	1580	0,45
56,6163	37,698	1600	0,46
56,8581	37,2718	1600	0,46
58,3691	37,2609	1600	0,46
58,4553	37,3972	1600	0,46
56,6463	37,7116	1610	0,46
57,316	37,3669	1650	0,47
57,3753	37,7467	1650	0,47
57,3908	37,7143	1650	0,47
57,4321	37,6677	1650	0,47
57,4787	37,6353	1650	0,47
56,9674	37,2957	1700	0,49
57,3976	37,3936	1700	0,49
57,4274	37,1478	1700	0,49
57,4735	37,6859	1700	0,49
57,5097	37,6576	1700	0,49
57,5691	37,617	1700	0,49
58,4488	37,4362	1700	0,49
58,5138	37,4232	1700	0,49
57,4964	37,7291	1800	0,51
58,3566	37,3237	1850	0,53
57,3941	37,1578	1900	0,54
57,7531	37,3722	1900	0,54
58,2876	37,4945	1900	0,54
58,3962	37,5094	1900	0,54
58,7863	37,3092	1930	0,55
57,4849	37,2029	2000	0,57
57,7095	37,4812	2000	0,57
57,7553	37,7102	2000	0,57
57,7889	37,6657	2000	0,57
57,8535	37,617	2000	0,57
57,9	37,5623	2000	0,57
56,2995	37,151	2050	0,59
56,183	37,3522	2060	0,59
57,7338	37,4093	2100	0,60
57,7614	37,3359	2100	0,60
58,3216	37,4014	2100	0,60
57,153	37,3488	2300	0,66
59,1918	37,2532	2400	0,69
58,0081	36,9752	2500	0,71
58,3435	37,5846	2500	0,71
58,5164	36,8055	2500	0,71
57,2031	37,3617	2600	0,74
57,3417	37,7325	2600	0,74
57,3675	37,69	2600	0,74
57,4063	37,6515	2600	0,74
57,42	37,4926	2600	0,74
57,4296	37,6231	2600	0,74
58,5205	36,7447	2600	0,74
58,6159	37,5664	2600	0,74
58,6243	37,2955	2600	0,74
56,1658	37,1124	2800	0,80
58,0215	37,6798	2800	0,80
58,0474	37,6373	2800	0,80
58,0887	37,6069	2800	0,80
58,1146	37,5623	2800	0,80
58,1585	37,5238	2800	0,80
58,6672	37,3938	2800	0,80
57,4907	38,2913	2900	0,83
57,5207	38,2604	2900	0,83
58,7109	37,2333	3000	0,86
58,0445	36,9773	3500	1,00
58,0908	36,9796	3600	1,03
58,5888	37,0846	4000	1,14
58,1903	37,4973	4100	1,17
58,1944	37,4635	4100	1,17
58,2057	37,3852	4100	1,17
57,7036	37,7386	4200	1,20
57,7268	37,7062	4200	1,20
57,7553	37,6535	4200	1,20
57,807	37,6089	4200	1,20
57,8483	37,5562	4200	1,20
57,9	37,4995	4200	1,20
57,9181	37,461	4200	1,20
57,6931	38,1479	4700	1,34
57,0211	38,4945	5000	1,43
57,0392	38,4662	5000	1,43
57,0521	38,4317	5000	1,43
57,0806	38,3912	5000	1,43
57,0987	38,3608	5000	1,43
57,6148	38,1852	5200	1,49
57,7475	38,0135	5200	1,49
57,5128	38,2403	5300	1,51
58,3646	37,5978	5500	1,57
57,0915	38,486	6000	1,71
57,114	38,4406	6000	1,71
57,1616	38,3925	6000	1,71
57,406	38,3545	7500	2,14
57,2535	38,4639	7800	2,23
57,338	38,4203	7800	2,23
58,43	37,5238	9200	2,63
58,4687	37,4812	9200	2,63
58,492	37,4407	9200	2,63
57,7966	37,8055	10 250	2,93
57,8406	37,7569	10 250	2,93
57,9052	37,7001	10 250	2,93
57,9569	37,6515	10 250	2,93
57,9957	37,5826	10 250	2,93
58,0448	37,5319	10 250	2,93
58,0629	37,4711	10 250	2,93
58,0784	37,4265	10 250	2,93
58,1172	37,3678	10 250	2,93

Longitude (°E)	Latitude (°N)	Offset (m)	Slip rate (mm yr^{-1})
58,3365	37,2842	11 000	3,14
57,838	37,8987	11 600	3,31
58,2128	37,465	12 700	3,63
58,249	37,4245	12 700	3,63
58,2645	37,386	12 700	3,63
58,2826	37,3475	12 700	3,63
57,9207	37,8237	14 500	4,14
58,0189	37,765	14 500	4,14
58,0862	37,6981	14 500	4,14
58,1275	37,6494	14 500	4,14
58,1508	37,6049	16 800	4,80
58,1766	37,5583	16 800	4,80
58,1999	37,5137	16 800	4,80
56,5688	38,7458	18 100	5,17
56,6179	38,7094	18 100	5,17
56,6799	38,679	18 100	5,17
56,7678	38,6465	18 100	5,17
56,8298	38,6161	18 100	5,17
56,8945	38,5797	18 100	5,17
56,9255	38,5432	18 100	5,17
56,9539	38,527	18 100	5,17